SF 298 MASTER COPY KEEP THIS COPY FOR REPRODUCTION PURPOSES

# REPORT DOCUMENTATION PAGE

*Form Approved OMB NO. 0704-0188*



| 1. AGENCY USE ONLY *(Leave blank)* | 2. REPORT DATE | 3. REPORT TYPE AND DATES COVERED |
|---|---|---|
| | **1/31/96** | Final 1 Aug 92 - 31 Jan 96 |

4. TITLE AND SUBTITLE
**EXPERIMENTAL STUDY OF UNUSUAL IR AND FAR IR VIBRATIONAL ENERGY TRANSFER PROCESSES IN SOLIDS**

5. FUNDING NUMBERS
DAAL03-92-G-0369

6. AUTHOR(S)
**A. J. Sievers**

7. PERFORMING ORGANIZATION NAMES(S) AND ADDRESS(ES)
**Cornell University**
**Laboratory of Atomic & Solid State Physics**
**Clark Hall**
**Ithaca, NY 14853-2501**

8. PERFORMING ORGANIZATION REPORT NUMBER

9. SPONSORING / MONITORING AGENCY NAME(S) AND ADDRESS(ES)
U.S. Army Research Office
P.O. Box 12211
Research Triangle Park, NC 27709-2211

10. SPONSORING / MONITORING AGENCY REPORT NUMBER
ARO 30155.31-PH

11. SUPPLEMENTARY NOTES
The views, opinions and/or findings contained in this report are those of the author(s) and should not be construed as an official Department of the Army position, policy or decision, unless so designated by other documentation.

12a. DISTRIBUTION / AVAILABILITY STATEMENT
Approved for public release; distribution unlimited.

12 b. DISTRIBUTION CODE



13. ABSTRACT *(Maximum 200 words)*

Seven different experimental studies are described.
(a) Hole burning in chalcogenide glasses: The dephasing time is a function of the average coordination number of the glass and is independent of the chemical composition.
(b) Vibrational relaxation of diatomic molecules in alkali halide crystals: The matrix isolated CN- molecule obeys an energy gap law while the hydride molecule does not.
(c) Vibrational relaxation of diatomic molecules in glass: Our IR pump-probe examination of SH in As2S3 glass has show that this impurity molecule is actually weakly hydrogen bonded in the glassy structure.
(d) Pocket vibrational modes in crystals: A systematic study of a point defect in a crystal lattice has demonstrated that there are localized modes with the maximum mode amplitude at sites far removed from the defect itself.
(e) Intrinsic localized vibrational modes in perfect crystals: The inclusion of both cubic and quartic terms in the potential has produced not only localized vibrational modes but also a localized dc expansion at the mode site.
(f) Extinction sum rules for particles of arbitrary size: We have uncovered a general extinction sum rule which is independent of the size of the particle in relation to the wavelength and independent of the composite nature of the particle.
(g) Measurement of a charged particle bunch from the coherent transition radiation mm-wave spectrum: The coherent far infrared radiation induced from relativistic electron bunches submillimeter length provides a new way to characterize the electron bunch shape.

| 14. SUBJECT TERMS | 15. NUMBER IF PAGES |
|---|---|
| Persistent IR spectral hole burning; dephasing time; chalcogenide glasses, glass coordination number; Vibrational relaxation; hydride molecules; IR pump-probe experiments; pocket vibrational modes; intrinsic localized vibrational modes; localized dc expansion; extinction sum rules; charged particle bunch; coherent mm-wave transition radiation. | **59** |
| | 16. PRICE CODE |

| 17. SECURITY CLASSIFICATION OR REPORT | 18. SECURITY CLASSIFICATION OF THIS PAGE | 19. SECURITY CLASSIFICATION OF ABSTRACT | 20. LIMITATION OF ABSTRACT |
|---|---|---|---|
| UNCLASSIFIED | UNCLASSIFIED | UNCLASSIFIED | UL |

NSN 7540-01-280-5500



Standard Form 298 (Rev. 2-89)
Prescribed by ANSI Std. 239-18
298-102

# EXPERIMENTAL STUDY OF UNUSUAL IR AND FAR IR VIBRATIONAL ENERGY TRANSFER PROCESSES IN SOLIDS

FINAL REPORT

A. J. SIEVERS

JANUARY 31, 1996

U. S. ARMY RESEARCH OFFICE

GRANT DAAL03-92-G-0369

CORNELL UNIVERSITY

THE VIEW, OPINIONS, AND/OR FINDINGS CONTAINED IN THIS REPORT ARE THOSE OF THE AUTHOR AND SHOULD NOT BE CONSTRUED AS AN OFFICIAL DEPARTMENT OF THE ARMY POSITION, POLICY, OR DECISION, UNLESS SO DESIGNATED BY OTHER DOCUMENTATION.

## Table of Contents

## I. SUMMARY

Our most significant discoveries made during the last three years in the different areas of optical physics are summarized below. These items are described in more detail in the body of the final report.

(a) Effects of Network Topology on Low-Temperature Relaxation in Ge–As–Se IR Transmitting Glasses: The discovery of persistent spectral hole burning in the infrared vibrational modes of simple molecular impurities in the chalcogenide glasses, the first instances of non-electronic persistent hole burning in covalently bonded glasses, makes available a powerful spectroscopic technique for the investigation of glassy dynamics in a particularly rich and versatile class of materials. Persistent hole burning has been observed for a diverse set of host–impurity combinations — including SH, $D_2O$, OD, and $CO_2$ in $As_2S_3$; $CO_2$ in glassy Se; and SeH in Se, $As_2Se_3$, and Ge–As–Se glasses — suggesting that vibrational hole burning is universal in the chalcogenide glasses. This new class of hole burning systems displays a wealth of intriguing behavior, including hole width temperature dependences ranging from $T^{1.3}$ for a–Se to $T^2$ for $As_2S_3$, and the erasure of holes by extremely small doses of band-gap light. Despite the disparate nature of the impurity centers, as underscored by the wide range of hole widths at 1.5 K (from 80 MHz for $CO_2$ in $As_2S_3$ and Se, to over 20 GHz for holes on the low frequency extreme of the SH stretch band in $As_2S_3$), different impurities in a given host display remarkably similar 1.5K spectral hole relaxation behaviors, lending credence to the idea that hole burning proceeds via configurational changes in the glassy matrix. Large variations in the hole relaxation behavior do occur, however, when a single type of impurity is placed in different hosts. To investigate a possible structural origin for this variation, the 1.5K relaxation of spectral holes burned in the 4.5μm SeH absorption band is studied as a function of network connectivity for a number of glass compositions in the Ge–As–Se system, with the striking result that the dominant rate characterizing the non-exponential relaxation increases monotonically by over three orders of magnitude as the average atomic coordination number of the host is increased from 2.0 to 2.8. Over the composition range studied the quantitative form of the non-exponential hole relaxation depends solely on the average coordination number, independent of chemical composition. By making a systematic study of the resulting vibrational hole shape across the Ge-As-Se glass series we have shown that the dephasing time is a function of the average coordination number or mean bond number of the glass and is independent of the chemical composition.

This is the first time that structural topology has been connected with the dephasing dynamics.

(b) Vibrational relaxation of diatomic molecules in alkali halide crystals: By measuring the vibrational lifetime of $CN^-$ in silver halides we were able to demonstrate conclusively that for simple crystals the vibrational lifetime of this molecule obeys an energy gap law; the farther the important lattice vibrations are from the stretch mode frequency the longer the vibrational lifetime. A systematic study of the vibrational lifetime of diatomic hydride molecules in simple crystals shows that they do not obey such an energy gap law. The reason for this dichotomy remains a mystery.

(c) Vibrational relaxation of diatomic molecules in glass: Our IR pump-probe examination of SH in $As_2S_3$ glass has show that this impurity molecule is actually weakly hydrogen bonded in the glassy structure. The stronger the hydrogen bonding at a site the lower the vibrational frequency and the shorter the molecules lifetime. The lifetimes determined by this direct (fast) measurement are the same as those previously inferred from the (slow) persistent hole burning technique demonstrating for the first time that both techniques can be used equally well to measure lifetimes.

(d) Pocket Vibrational Modes in Crystals: A systematic study of the vibrational energy levels induced by a point defect in a crystal lattice has demonstrated that there are localized modes with the maximum mode amplitude at sites far removed from the defect itself. In the past it has always been assumed that defect modes would be localized at the impurity site. The discovery of such pocket modes may help to explain the high mobility of the $Ag^+$ ion in some crystal lattices.

(e) Intrinsic Localized Vibrational Modes in Perfect Crystals: Our numerical investigation of nonlinear 1-D lattices has continued to support the hypothesis that intrinsic localized vibrational modes are a natural feature of perfect anharmonic lattices. The inclusion of both cubic and quartic terms in the potential has produced not only localized vibrational modes but also a localized dc expansion at the mode site. When the localized mode moves through the lattice it is accompanied by this localized dc expansion giving the excitation an effective translational mass.

(f) Uncovering Extinction Sum Rules for Particles of Arbitrary Size: Our investigation of the far infrared properties of simple dielectric composite structures such as hot pressed ZnS+diamond particles has produced a number of new ideas for the analysis of the optical properties of such complex structures. Most interesting is that we have uncovered a general extinction sum rule which is independent of the size of the particle in relation to the wavelength and independent of the composite nature of the particle.

(g) Measurement of the longitudinal asymmetry of a charged particle bunch from the coherent synchrotron or transition radiation mm-wave spectrum: The coherent far infrared radiation induced from relativistic electron bunches of millimeter and submillimeter length provides a new way to characterize the electron bunch shape. Once the spectrum associated with the bunch form factor is measured a Kramers-Kronig relation is applied to the spectral form factor to find the minimal phase and then the bunch shape is determined from the complete Fourier transform. Our successful demonstration of this idea has given us access to high peak intensity, psec pulses of mm-wave radiation from the Cornell linac.

## II. PROGRESS

### A. Effects of Network Topology on Low-Temperature Relaxation in Ge–As–Se IR Transmitting Glasses

1. Persistent spectral hole filling

Our discovery of persistent infrared spectral hole (PIRSH) burning in sulfur–hydrogen vibrational mode in the infrared transmitting glass $As_2S_3$ [1] represented the first instance of non-electronic spectral hole burning a covalently bonded glass. As more impurity centers were successfully prepared in chalcogenide glasses, it became clear that the $As_2S_3$:SH system was not an anomaly, but rather was the first example of a whole new class of hole burning systems.

In monitoring the time evolution of the spectral hole after burning ceases, one is in effect monitoring the relaxation among the glassy configurations involved in the hole burning. Experiments of this type have been performed by many workers on a variety of amorphous systems, both organic and inorganic [2-4]. The one qualitative feature universal to all these systems is the highly non-exponential nature of the hole relaxation, indicating the existence of a broad distribution of relaxation rates for each system. Quantitatively, however, these distributions of relaxation rates vary widely from system to system, with the most probable relaxation rate varying by several orders of magnitude. Until now, the diverse nature of the systems studied has made meaningful correlations between glass structure and hole relaxation behavior impossible.

This situation changed with the discovery that persistent infrared spectral holes burned in the SeH vibrational absorption band display radically different relaxation behavior in glassy Se and $As_2Se_3$. That two glasses which seem to be quite similar in other respects should exhibit spectral holes for which the dominant relaxation rates differ by nearly three orders of magnitude is quite surprising. The obvious difference between these two glasses is that Se glass consists of weakly interacting chains of two-fold coordinated Se atoms, while in $As_2Se_3$ these chains are cross-linked by three-fold coordinated As atoms. This result suggested a relation between the microscopic topology of the glass network and hole relaxation behavior, but chemical effects due to the presence or absence of As could not be ruled out. The importance of this result, however, is that both glasses are members of a large class of glass-forming alloys which allow continuous variation of structure by varying alloy composition, opening the way for a systematic study of the effects of network topology on spectral hole behavior.

The ternary Ge–As–Se system is particularly well-suited to exploring the role of topology in determining relaxation behavior because its large glass-forming region makes it possible for a given value of the average coordination number <r>, a key parameter for describing network connectivity, to be realized with a continuous range of chemical compositions, allowing purely topological effects to be distinguished from chemical effects. The basic way in which the microscopic network

structure of a chalcogenide glass is determined by its composition is illustrated schematically in Fig. 1 for the specific case of Ge–As–Se glasses. It is energetically favorable for a chalcogen atom such as Se to have two covalent bonds per atom, a condition in which it is said to be two-fold coordinated. Elemental Se glass is thus made up of chains of Se atoms as in Fig. 1 (a), each Se within a chain covalently bonded to two others, and weak Van der Waals interactions providing the only coupling between chains. The result is a loose, non-rigid structure. This structure can be modified by replacing some of the Se atoms with As or Ge atoms, which prefer to be three-fold and four-fold coordinated, respectively. The result of adding these higher coordination atoms, as shown in Fig. 1 (b), is to cross-link the Se chains, adding rigidity to the structure. In this picture, then, the larger the Ge or As fraction is, the more rigid the structure, leading to such

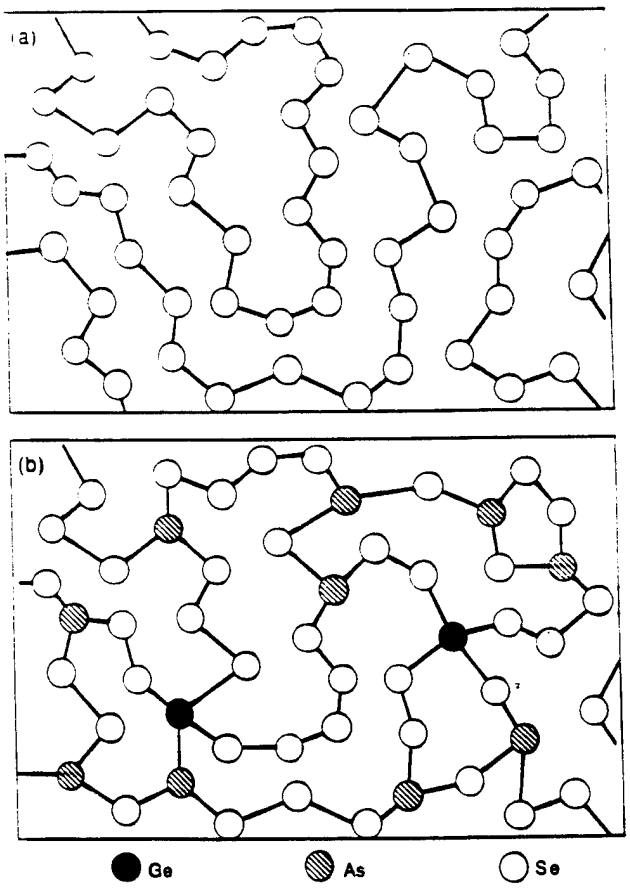


Figure 1. Schematic representations of the structure of elemental Se and Ge–As–Se glasses. (a) Elemental Se glass. The two-fold coordinated Se atoms form chains with strong covalent bonds between the Se atoms within a given chain and only weak interactions between chains, producing a low rigidity structure. (b) Ge–As–Se glass. Replacing two-fold coordinated Se atoms with three-fold coordinated As or four-fold coordinated Ge has the effect of cross-linking the Se chains, adding rigidity to the network structure.

observable differences as larger elastic constants and higher glass transition temperatures. The question now is how to express this picture in a quantitative fashion.

The role of microscopic topology in determining the properties of glass-forming compounds has been explored theoretically for several years. Phillips[5,6], in constraint counting arguments attempting to explain the strong glass-forming tendency of certain alloy compositions, first suggested that the network connectivity could be parameterized by simply using an average atomic coordination number, <r>, where r is the coordination number of each atom in the glass, i.e. the number of neighboring atoms covalently bonded to that atom. The idea is then to replace the real network structure, consisting of a variety of atoms of different coordination numbers, with a network of identical virtual atoms, all having the coordination number <r>. The distinguishing feature of this approach, as opposed to ball-and-stick type mechanical models, is that it permits non-integral coordination numbers, and recognizes the topological relevance of such a concept.

These ideas were futher refined by Thorpe et al.[7-9] and Tanaka.[10] who argued that as <r> is increased, rigid regions form in the "floppy" structure of pure Se glass, growing in size and number until at some critical value of <r> the rigid regions become connected throughout the network; i.e., a "rigidity percolation" transition occurs from an underconstrained "floppy" structure to an overconstrained rigid structure. This rigidity percolation, it is argued, should occur when the number of floppy modes goes to zero which for the above system occurs at $r_p = 2.4$ .

The key parameter in relating the properties of the glass-like solids to their microscopic topology rather than to their chemical nature is the mean coordination number <r>, i. e. the average number of covalent bonds per atom. Because the chalcogenides are such good glass formers over a wide range of alloy composition[11], they offer a promising system for testing these ideas. In the GeAsSe compounds, each Ge atom has four, each As atom three and each Se atom has two covalent bonds, thus the mean coordination number <r> for a GeAsSe alloy is simply calculated from the concentration of the three constituents according to

$$< r >= 4 \cdot [Ge] + 3 \cdot [As] + 2 \cdot [Se]. \qquad (1)$$

By studying hole filling as a function of time for a single molecular impurity in the Ge-As-Se glass series we have found that large variations in the hole relaxation behavior do occur. To investigate a possible structural origin for this variation, the 1.5K relaxation of spectral holes burned in the 4.5μm SeH absorption band has been studied as a function of network connectivity for ten glass compositions in the Ge–As–Se system, with the striking result that the dominant rate characterizing the non-exponential relaxation increases monotonically by over three orders of magnitude as the average atomic coordination number of the host is increased from 2.0 to 2.8. Therse results are shown in Fig. 2.

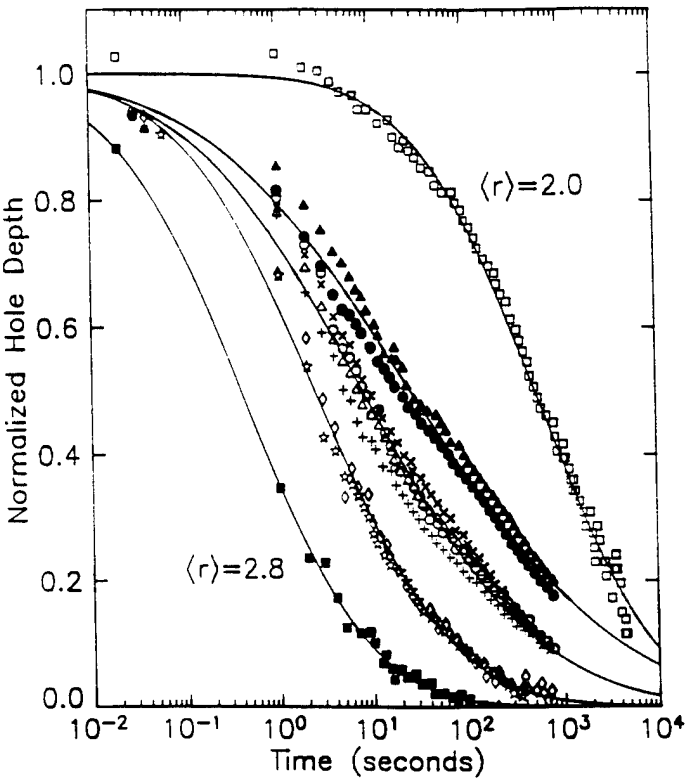


Figure 2. Spectral hole refilling at 1.5 K for the SeH absorption in Ge–As–Se glasses. Data points show the hole depth, normalized to unity at t=0, as a function of time t after burning ceases for ten different compositions burned and probed under identical conditions. The laser frequency is 2227 $cm^{-1}$ and the intensity at the sample is roughly 200 $mW/cm^2$. The initial hole in each sample is burned for 2 minutes. The average atomic coordination numbers $< r >$ and compositions of the ten samples, listed in order of decreasing relaxation time, are as follows: $< r > = 2.0$ — glassy Se (open squares); $< r > = 2.2$ — $As_{0.2}Se_{0.8}$ (solid triangles), $Ge_{0.089}As_{0.022}Se_{0.889}$ (solid circles); $< r > = 2.4$ — $Ge_{0.15}As_{0.10}Se_{0.75}$ (x), $As_2Se_3$ (open circles), $Ge_{0.1}As_{0.2}Se_{0.7}$ (open trianlges), $Ge_{0.133}As_{0.133}Se_{0.733}$ (+); $< r > = 2.6$ — $Ge_{0.1}As_{0.4}Se_{0.5}$ (open diamonds), $Ge_{0.2}As_{0.2}Se_{0.6}$ (open stars); $< r > = 2.8$ — $Ge_{0.3}As_{0.2}Se_{0.5}$ (solid squares). Solid lines are fits, for each set of compositions having a given value of $< r >$, to a Gaussian distribution of tunneling parameters.

The remarkable result of these experiments is that the hole relaxation behavior in these glasses appears to be determined solely by network connectivity considerations, independent of chemical composition.

2. Dephasing properties of molecules in chalcogenide glass

Because of the advance of laser spectroscopic techniques such as fluorescence line narrowing, persistent spectral hole burning and the photon echo, the temperature dependence of homogeneous optical line widths of atoms and molecules in glasses has been the subject of many experimental investigations in recent years[1,12-19]. The dephasing rate of a defect in a glass at low temperature is orders of magnitude larger compared to its counterpart in a crystal and the temperature

dependence of the homogeneous linewidth is significantly different in crystals and glasses. The dephasing rate in crystals is fairly well understood: a Raman process with phonons gives rise to a $T^7$ -dependence at low temperatures if the phonon modes are not strongly perturbed by the defect while if they are perturbed an exponential law results due to interaction of the optical center with local modes. Above the Debye temperature a quadratic temperature dependence due to interaction with phonons in a Raman process is found. For the dephasing rate in glasses the homogeneous line width is characterized by a power law[20-22]. The experimental temperature dependence for both organic and inorganic glasses is given by[15-17]

$$\Gamma_{hom}(T) = \Gamma_{hom}(T = 0) + a \cdot T^b \qquad (2)$$

with the exponent b somewhere between 1 and 2.3 down to the lowest temperatures[3,13,15-17,23].

Glasses seem to fall roughly into two categories. Organic systems show an approximately linear temperature dependence of the homogeneous linewidth with an exponent b near 1.3 while inorganic materials are typically characterized by a quadratic power law although variations in b from 1.3 to 2.3 are found. To date the temperature exponents measured with fast and slow methods are basically the same even though the measured widths themselves may be different[3,18,23]. Although there is a consensus that the two level systems of glasses[24,25] are important, the detailed dynamical picture is unclear. Most dephasing theories[13,26] explain the larger homogeneous widths and their anomalous temperature dependence in terms of the interaction of the impurities with a broad distribution of two-level systems. If the nature of the interaction of the two-level systems with the optical center is assumed to be dipolar then, according to some theories[13,26,27], the temperature exponent of the homogeneous linewidth is $1+\mu$, where $\mu$ is the exponent that characterizes the density of two level systems which is $\propto E^{\mu}$ as a function of their energy splitting E. It is found in thermal experiments[28] that $\mu = 0.3$, so that the temperature exponent of the homogeneous linewidth comes out to be 1.3 in accordance with many of the experimental findings in organic glasses. Other theories, which invoke "fractons" [29] or "tunnelons"[30] have also been proposed to explain dephasing processes in glasses. To explain the findings in inorganic glasses, Huber[31,32] has proposed a two phonon Raman process as the dephasing mechanism with an effective Debye temperature which is 2 to 10 times lower in glasses than their nominal value in crystals. The density of low lying vibrational modes has been measured by neutron scattering in vitreous silica and found to be larger than the Debye value[33]. This leads to an extention of the quadratic temperature dependence to lower temperatures but there are data at temperatures much below this effective Debye temperature which do not show a transition to the expected $T^7$ dependence[32,34,35].

In all of the fluorescence line narrowing, persistent spectral hole burning and photon echo studies of organic and inorganic glass, it is still not clear how much of the underlying behavior is controlled by chemical bonding and how much by local glass structure because little work has been carried out on systems in which the chemistry can be varied in a systematic manner. As mentioned above for the chalcogenide glass the constraint counting arguments[5-10] lead to topological thresholds at $\langle r \rangle = 2.4$ and $\langle r \rangle = 2.67$. Both have been observed in different glasses as extrema or kinks in physical properties as a function of the mean coordination number, such as the glass forming temperature, the mean atomic volume, the dielectric constant, the thermal diffusivity or the fragility[36-39]. We have found a supporting correspondence in the time dependent systematics of the hole filling properties[4] as described above.

Until our work below there existed no systematic study of a possible connection between the glass structure and the temperature dependence of optical line widths because the chalcogenide glasses are opaque in the visible where most of the temperature dependent line width investigations have been performed[12-17]. Persistent IR spectral hole burning in the electronic ground state first observed for SH in $As_2S_3$ glass[40] was quickly generalized to other molecules in chalcogenide glasses[1] since all the GeAsSe glasses are transparent in the infrared region of the spectrum. Here we describe our measurements of the temperature dependence of the hole width and show that they follow a power law in temperature for all samples. Our general result is that the temperature exponent in Eq. (2) increases with increasing mean coordination number $\langle r \rangle$ of the glass indicating that structural topology also plays a role in the temperature dependence of the dephasing time.

A schematic optical layout for the hole burning experiment is shown in Fig. 3. The radiation source is a lead-salt diode laser mounted on the cold finger of a closed cycle refrigerator. Rough frequency tuning is achieved by changing the operation temperature of the diode whereas the fine tuning is done by controlling the laser current. For the experiments described here the laser is operated at a center frequency of 2230 $cm^{-1}$ (4.48 μm ), which is coincident with the high frequency wing of the inhomogeneous SeH-line of *all* samples and allows us to perform the hole burning using the same laser mode. The high frequency side of the absorption band is chosen because the holes here are much narrower and depend much less strongly on frequency compared to the low frequency side of the inhomogeneous absorption line[1,41]. The center frequency of the laser is determined with a Jarrell-Ash 3/4 meter monochromator with a 50 line/mm grating.

3. Dependence of the line width on the mean coordination number

For two different temperatures the hole width dependence on the mean coordination number is shown in Fig. 4. At T = 0 K there is an increase in this width from about 0.5 GHz to 1.5 GHz over the range of mean coordination numbers from 2.0 to 2.6. Only the data point at $\langle r \rangle = 2.4$ doesn't follow the increasing tendency but indicates a minimum at this value. Note that a rigidity

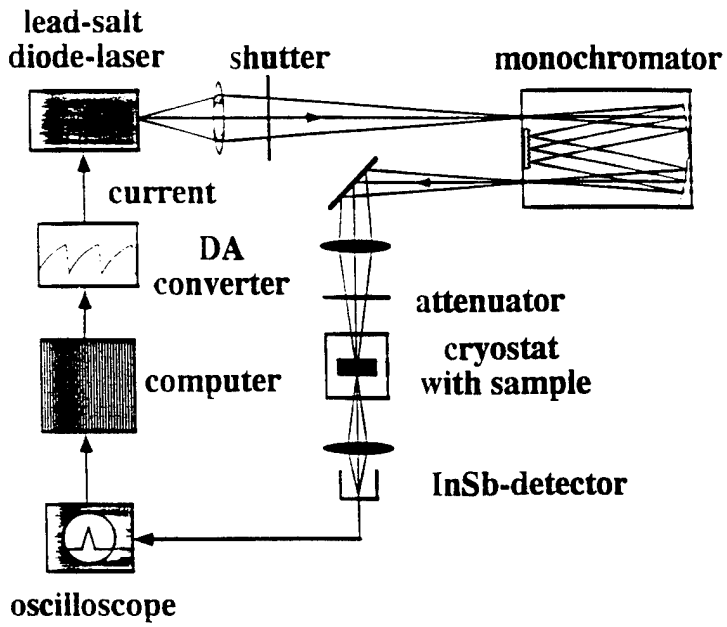


Figure 3. Experimental setup for persistent IR spectral hole burning experiments.

transition is expected to occur at glasses with this average number of bonds per atom [7] Assuming that the widths at zero temperature are lifetime limited, the correspondent lifetimes $T_1$ of the SeH-vibration vary from 0.3 ns to 0.1 ns. The width measured at approximately 40K also is shown in Fig. 4. It drops continuously with increasing coordination number from a value of 11 GHz at r = 2.0 to approximately 5 GHz at r = 2.6. This different dependence may be a consequence of the role of the dephasing time in the hole width at elevated temperatures.

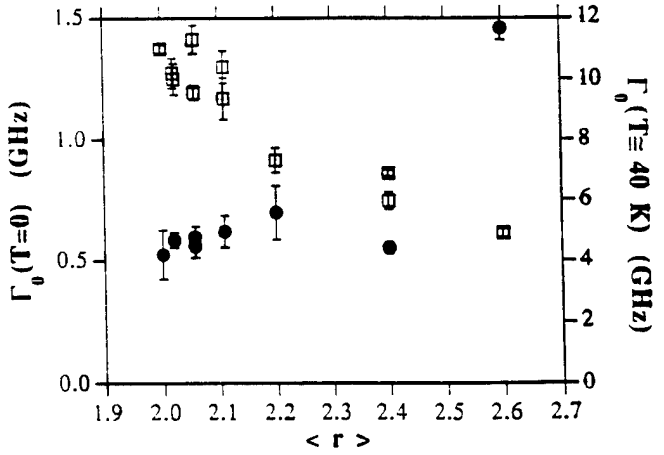


Figure 4. Dependence of the low temperature homogeneous hole width on the mean coordination number < r >. Solid circles and left scale: hole width extrapolated to zero temperature. Open squares and right scale: hole widths at T = 40K.

In Figure 5 the results for the temperature exponent b are displayed as a function of the mean coordination number <r>. Figure 5 shows the temperature exponent at FWHM range from 1.5 to 2.0. The smallest value is measured at a mean coordination number <r> = 2.0, i.e. in the pure Selenium sample. With increasing coordination number the temperature exponent rises, the strongest between mean coordination numbers 2.0 and 2.1. Notice that although the compositions of sample no. 3 and no. 4 are different. their mean coordination number is the same (<r> = 2.057) and so is the result for the temperature exponent.

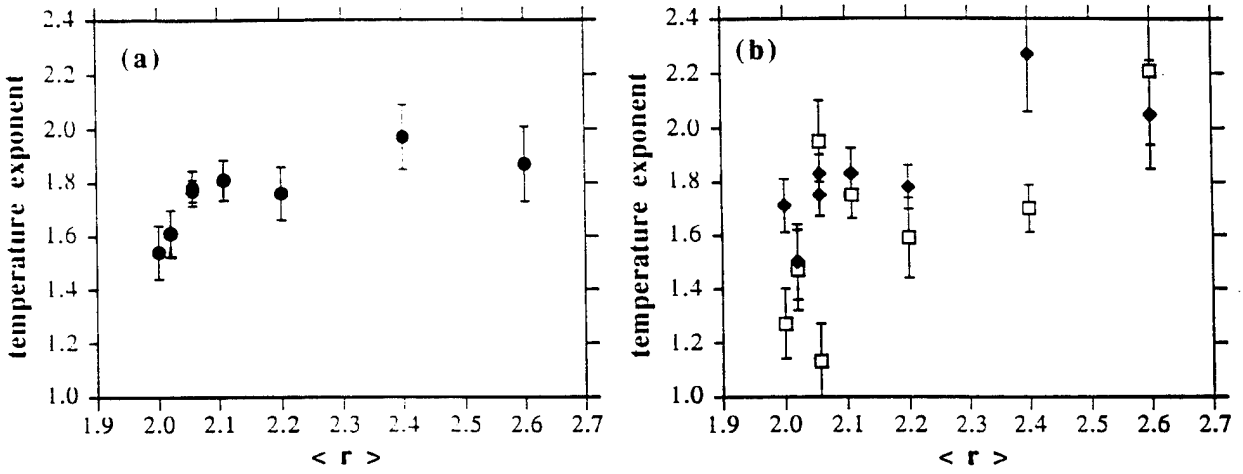


Figure. 5. Temperature exponent b versus mean coordination number < r >.
(a) Data corresponding to evaluation at FWHM.
(b) Data corresponding to evaluation at 3/4 of the maximum are plotted as solid diamonds; data corresponding to evaluation at 1/4 of the maximum as open squares.

We speculate that the increase in the temperature exponent with <r> might be connected to a transition of the purely chain like structure of the Selenium to a higher dimensional structure. According to the model proposed by Phillips[5,6] the structure in the GeAsSe glasses consists mainly of one dimensional units for 2 < <r> < 2.06. In the region between 2.08 and 2.18 cross linking of the Se-chains by fourfold coordinated Ge and threefold coordinated As atoms leads to the development of structures with two-dimensional character and above that value to three dimensional clusters. These ideas are supported by measurements of the viscosity of $As_xSe_{1-x}$ and $Ge_xSe_{1-x}$ glasses[42]. They show significant drops in the entropy of activation for viscosity at r = 2.08 and 2.18. The first value coincides with the transition from a sharp rise to a flatter <r> dependence of the temperature exponent in our experiment. The transition to structures with higher dimensions doesn't seem to influence the temperature exponent significantly. There is no indication of any change in the exponent at the customary topological thresholds at <r> = 2.4 or 2.67.

The dephasing of optical centers in glasses at low temperatures has been attributed to an interaction with two level systems which leads to a power law in the temperature dependence of the homogeneous linewidth. If the density of two level systems varies with energy as $\varepsilon^{\mu}$ and the strength of the interaction as $r^{-n}$, the temperature exponent[43] is given by $(1+\mu)\ n/3$. For a dipole-dipole interaction n=3, for a dipole-quadrupole interaction n=4, etc. Within the framework of this model, a systematic increase of the temperature exponent may indicate that either $\mu$ or n increases with mean coordination number. If one assumes that $\mu$ remains constant since it is a universal property of glasses and has the value 0.3 as found from thermal experiments in other glasses, the increase of the temperature exponent from 1.5 to 2.0 leads to an increase in n from 3.5 to 4.6. These values may indicate that already in pure Se the interaction between two-level systems and the optical centers is of higher order than dipolar. Note that the resulting interact would then be consistent the non-Lorentzian shape of the observed hole spectra. On the other hand, it is difficult to explain within the framework of this model why most of the change in the temperature exponent shown in Fig. 5 would occur in the range $2 < \langle r \rangle < 2.1$.

In summary we have performed persistent infrared spectral hole burning experiments on the inhomogenously broadened vibrational stretch band of SeH-defects in GeAsSe glasses over the temperature range from 1.5 to 50 K. The sample compositions were varied to systematically investigate the influence of the mean coordination number between r = 2.0 to r = 2.6 on the dephasing time. The observed widths in this limit follow a temperature dependence according to $\Gamma_0 + a\,T^b$. The temperature exponent b is found to increase with mean coordination number from 1.5 at $\langle r \rangle = 2$ to 1.9 at $\langle r \rangle = 2.6$. In the same range of coordination numbers the width at zero temperature $\Gamma_0$ shows a tendency to increase, which is interrupted by a possible minimum at r = 2.4. This result suggests that the lifetime of the mode also depends on $\langle r \rangle$. All of these findings suggest that the microscopic topology of the glass plays a significant role in determining the vibrational mode relaxation dynamics.

## B. Vibrational relaxation of diatomic molecules in alkali halide crystals

### 1. Host dependent lifetime of the CN ion

At low concentrations, a diatomic molecular impurity in a crystalline lattice whose internal vibrational mode is high in frequency relative to the host phonon bands is generally expected to decay radiatively at low temperatures, since nonradiative multiphonon relaxation constitutes an unlikely large-order process. This expectation is borne out in the cases of[44-46] CO and of NO in rare-gas matrices[44-46] . The 4.8 $\mu$m (2080 $cm^{-1}$) vibrational stretching mode of $CN^-$ doped in a number of different alkali halides [47-52] decays mainly radiatively at low temperatures with a lifetime on the order of 10 ms, in contrast to the ~5 ps nonradiative vibrational relaxation time measured for $CN^-$ in aqueous solution [53]. Although a diatomic has only one normal mode of

vibration, thus avoiding the complex issue of rapid energy redistribution among the internal modes of a polyatomic molecule, it is clear that an enormous range in relaxation times can nevertheless occur for the same diatomic molecule in different environments. Here we present the first measurements of the vibrational lifetimes of $CN^-$ in silver halides, finding times intermediate between those in the potassium, rubidium, and cesium halides and those in water. In seeking to understand the origin of the nonradiative decay channel for cyanide in the silver halides, we have discovered the existence of two local modes at 182 (207) $cm^{-1}$ and 299 (317) $cm^{-1}$ for $CN^-$ in AgBr (AgCl). By supposing that the stretching vibration is decaying into an appropriate number of these localized phonon modes, we can rationalize the relaxation rates of $CN^-$ in all of the solids with a single scheme: an energy gap law in which the highest-frequency bulk or localized phonons, as appropriate, constitute the dominant accepting modes. This model predicts that NaCl and NaBr must also have high-frequency local modes, in order to explain their short relaxation times (a few hundred microseconds), and these modes are in fact found.

Furthermore, we can explain the picosecond relaxation found for $CN^-$ in water, by assuming that the internal vibrations of the host molecules provide a near-resonant accepting mode. Extrapolating the energy gap law down to a single accepting mode gives a sub-nanosecond lifetime, in good agreement with the observed lifetime, especially in light of the fact that we have not made any corrections to the coupling parameters in the energy gap law.

This explanation for the rapid vibrational decay of the cyanide via coupling into local modes clears up a 10-year-old puzzle regarding the relaxation of $CN^-$ in the sodium halides. In these hosts, it was found that the low-temperature decay times are only a few hundred microseconds [54], in striking contrast to what was found for $CN^-$ in other alkali halides, but very similar to what we have found in the silver halides. Our measurements of the sideband spectra of samples of 0.5 mol % $CN^-$ in NaCl and NaBr show a line at +304 (+262) $cm^{-1}$ in NaCl (NaBr), which has the same width and temperature dependence as the local mode sidebands found in AgCl and AgBr. Thus, it is reasonable to also identify it as a local mode in this case [55].

In Fig. 6(a) the low-temperature relaxation times $\tau$ have been plotted versus the number of accepting modes N. For the alkali halides, these times were obtained by extrapolating the plateau in Lüty's data [54] at around 100 K down to zero temperature. This corrects for the low-temperature rise in his observed decay times, which we attribute to reabsorption of the $1 \rightarrow 0$ photons with a consequent bottleneck in the propagation of light out of the samples. (By about 100 K, this is no longer a problem because the $0 \rightarrow 1$ absorption is substantially weakened and the relaxation becomes increasingly nonradiative.) The highest-frequency accepting mode possible has been used for each host in the figure, i.e., the LO phonon frequency [56] in the case of the potassium, rubidium, and

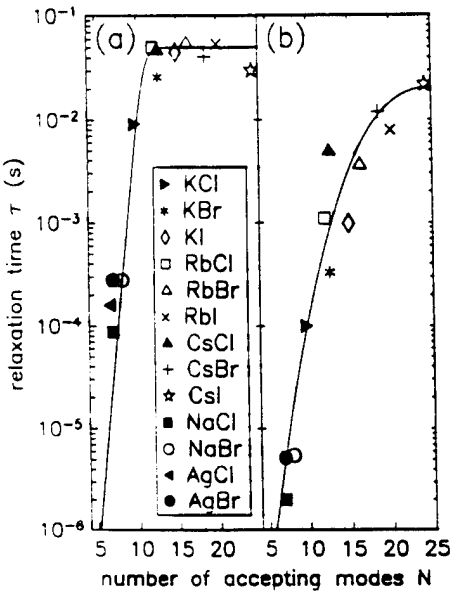


Figure 6. Relaxation times for the 1→0 vibrational decay of $CN^-$ in the indicated hosts at (a) 1.7 K, and (b) 300 K. The lifetimes of the silver halides were obtained by sideband pumping and/or by doubling the times found by overtone pumping. The accepting mode frequency, used to calculate the number of modes which match the vibrational energy, was chosen to be the LO phonon frequency [56]for the potassium, rubidium, and cesium halides, and the highest-frequency local mode for the sodium and silver halides.

cesium halides and the highest-frequency local mode in the case of the sodium and silver halides. The overall relaxation time $\tau$ is predicted to be

$$\tau = \left(1/\tau_{rad} + 1/\tau_{nonrad}\right)^{-1}, \tag{3}$$

where the radiative lifetime is $\tau_{rad}$ = 50 ms [47] and the nonradiative lifetime $\tau_{nonrad}$ is given by Eq. (1) at low temperatures. At high temperatures, it is necessary to modify Eq. (1) to include the temperature dependence expected for N accepting modes [57]:

$$\tau_{nonrad}(T) = \tau_0 e^{BN} \frac{\left(e^{h\nu_{acc}/kT} - 1\right)^N}{e^{h\nu_{vib}/kT} - 1}. \tag{4}$$

The fraction is equal to unity in the limit as T→0, so that this equation correctly reproduces Eq. (2) at low temperatures. The curves in Figs. 6(a)-(b) are plots of Eq. (3) after substituting Eq. (4), both fitted with the values $\tau_0$ = 50 ps and B = 1.93. Considering that B only depends logarithmically on the coupling constant and on N [44] , any variations of B from host to host are expected to be small enough to justify fitting the data, within experimental error, with a constant value of B. Furthermore, at 300 K, where the relaxation is largely nonradiative, the same value of B fits both bulk and localized phonon accepting modes, indicating that their vibrational couplings to $CN^-$ must

be similar (again on a logarithmic scale), which can be understood as follows. Consider the vibrationally-induced displacements of the host atoms surrounding the impurity: in the bulk accepting mode case, this distortion can be described as a superposition of phonons which subsequently propagate away from the defect in all directions; in the local mode case, a similar superposition of host atom displacements occurs, the difference being that the distortion subsequently remains localized.

If we extrapolate the curve in Fig. 6(b) down to a single accepting mode, we obtain a relaxation time of a few hundred picoseconds, 9 orders of magnitude smaller than the radiative lifetime of $CN^-$. Interestingly enough, this is not too different from the relaxation time measured for $CN^-$ in water [58], particularly if one makes allowance for the fact that the cyanide coupling constant in water would be expected to be somewhat different than that in salt crystals. This suggests that a $CN^-$ stretching mode is exchanging energy with a single nearly-resonant internal vibration of the water molecules.

In conclusion, the $2 \rightarrow 1$ vibrational relaxation times of $CN^-$ in AgCl and AgBr have been measured by overtone pumping and have been found to be 80 μs and 170 μs, respectively, at 1.7 K. This is roughly 1000 times faster than the times measured for $CN^-$ in the potassium, rubidium, and cesium halides. Two local modes for the cyanide-doped silver halide systems have been discovered and shown to be coupled to the $CN^-$ stretching mode by sideband pumping; the higher-frequency one at about 310 $cm^{-1}$, well above the host LO phonon frequencies, gives rise to an enhanced relaxation rate according to an energy gap law. This model correctly predicts that NaCl and NaBr must also have cyanide impurity local modes, since their relaxation times are comparable to those of the silver halides. By choosing the highest-available-frequency lattice or localized phonon to be the accepting mode, a temperature-dependent energy gap law successfully rationalizes the data for cyanide in all of the solids. The fitted law, furthermore, explains why the relaxation of $CN^-$ in aqueous solution occurs on a sub-nanosecond timescale, because the internal vibrations of the water molecules constitute an effective nearly-resonant accepting mode.

2. Ultrafast vibrational relaxation of diatomic hydrides

In contrast, with the CN- ion above our measurements[59] of the vibrational relaxation of $OH^-$ and $SH^-$ in the potassium halides indicate lifetimes on the order of 1 ns, much shorter than the radiative limit of ~50 ms. This agrees with the experimentally-determined upper limit of 5 ns on the $SH^-$ nonradiative lifetime, deduced previously from the lack of $2 \rightarrow 1$ vibrational fluorescence, following $0 \rightarrow 2$ overtone pumping.[60] These results are extremely surprising, since the stretching modes of these hydrides are even higher in frequency than those of $CN^-$ in the same hosts, and hence a higher-order multiphonon-relaxation process is anticipated.

An alternative nonradiative decay channel open to select systems is vibrational relaxation into rotations of the impurity. The first workers to advance such a model were . In 1975, Brus and Bondybey [61] studied vibrational relaxation within excited electronic manifolds of OH and OD in crystalline Ne at 4.2 K. They found that the $\upsilon$=1→0 relaxation rate is 2.3 times *faster* for OH than for OD. Noting that this contradicts a multiphonon-relaxation model, they proposed that the vibration decays into nearly-free rotations. Matching the vibrational transition, $\nu_{01}$, to the rotational energy requires $\nu_{01} = BJ(J+1)$, where $B$ is the rotational constant and $J$ is the rotational quantum number of the accepting level. Neglecting the factor of 1, since the rotational quantum number is large, gives

$$J \approx \sqrt{\nu_{01} / B} \tag{5}$$

(with a bulk phonon taking up the difference in the event that the right-hand side is non-integral). But the stretching frequency is proportional to the inverse root of the reduced mass of the molecule, whereas the rotational constant is proportional simply to the reciprocal mass via the moment of inertia. Hence, $J \propto (\mu)^{1/4}$ and OD is predicted to be a ~20% higher-order process than OH, explaining its slower relaxation. Similar measurements[62,63] and conclusions were made for NH and ND in Ne, Ar, and Kr. Minimal temperature dependence of the vibrational lifetimes was found for this latter case between 4.2 and 37 K, further ruling out multiphonon decay. For rotations the spacing between adjacent levels is strongly non-uniform and the temperature dependence is controlled by a few low-frequency transitions and hence is expected to be much weaker.

Other molecules in rare gas matrices which exhibit an isotope effect opposite to that predicted by a multiphonon decay model include HCl/DCl and $CH_3F/CD_3F$. Beginning with the former, it is generally believed[64,65] that these molecules exhibit weakly-hindered rotations in low-temperature Van der Waals matrices. The vibrational relaxation has been measured.[66,67] Fairly recent results[68] on $BH_2D_2^-$, which is similar in structure to $CH_3F$ but which was doped into the ionic alkali-halide matrices instead of the rare gases, indicate the existence of an efficient nonradiative decay channel. Since this molecule is both light and has a small moment of inertia, high-frequency local translational and librational modes arise, into which the vibrational energy was proposed to relax.

Over the last grant period, a comprehensive study of the vibrational relaxation of the diatomic chalcogen hydrides in the alkali halides was carried out. In addition to extending the $OH^-$ and $SH^-$ measurements to several additional hosts, new results are presented for $OD^-$ and $TeH^-$. A total of 18 different systems are measured and the vibrational relaxation times, $T_1$, are found to vary from 0.3 to 3 ns. The lack of a significant $OH^-$ isotope effect in the relaxation time upon deuteration, in particular, rules out a multiphonon-decay model, as the deuterated species is a factor of 1.357

(approximately $\sqrt{2}$) closer in frequency to the host phonon bands than is the hydride, and hence its relaxation process would be that much lower order. Assuming that the vibration-to-phonon coupling constants for the two isotopes are identical, one would then have expected an exponentially-faster decay rate for $OD^-$ compared to $OH^-$, in contrast to experiment. On the other hand, spectroscopic measurements indicate the existence of a superoptic local mode, identified as a librational mode of the molecule about its center of mass.[59,69,70] An energy gap law is found to describe the relaxation of the vibrations into these reorientational modes, using one set of coupling constants for all of the chalcogen hydrides. These results are shown in Fig. 7. One surprising result is that the coupling appears to be much stronger for these molecules even though the high frequency accepting modes both occur at about the same frequencies as for CN- in silver or sodium halides.

Unexpectedly, the vibrational relaxation times of the stressed crystals are not very different from those of their unstressed counterparts. For example, $SH^-$ at a substitutional site having only $I^-$ neighbors on its nearest <110> positions is found to have the same lifetime as that of $SH^-$ at a crystalline site wherein one of these neighbors has been replaced by a $Br^-$ ion. This relative

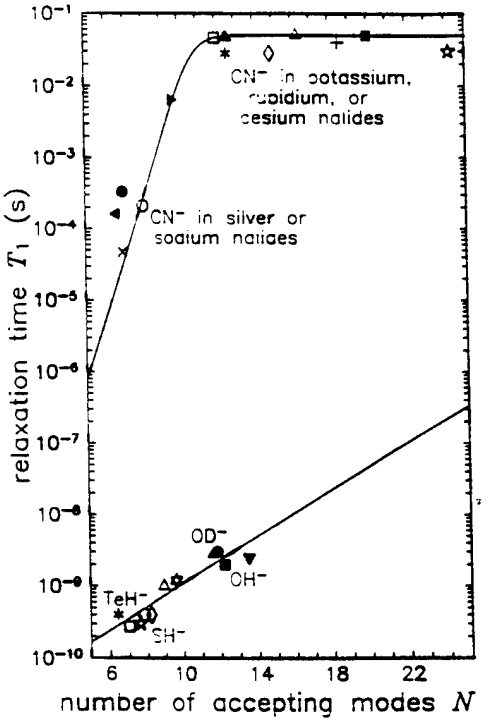


Figure 7. Comparison of the 1→0 vibrational relaxation times (symbols) of $CN^-$ and of $XH^-/XD^-$ in the alkali and silver halides at 1.7 K. The abscissa gives the ratio of the vibrational frequency to the accepting mode frequency, defined to be the longitudinal-optic phonon frequency for $CN^-$ in the potassium, rubidium, and cesium halides, the highest-frequency localized-translational mode in the case of $CN^-$ in the silver and sodium halides, and the librational frequency for the chalcogen hydrides.

insensitivity of the decay rates to the immediate local environments of the diatomics suggests that the coupling between the molecules and the lattice is weak. Yet this is difficult to reconcile with the fact that the the relaxation is fast: specifically, the decay of $SH^-$ into reorientational modes is found to be orders of magnitude faster than the decay[71] of $CN^-$ in the sodium and silver halides into an equivalent number of translational modes. If the coupling for the hydrides were weak, much slower relaxation would be expected.

Also surprising is the discovery that the assigned librational mode disappears with increasing temperature. This evolution can be seen most easily by examining the sideband spectrum associated with the stretch vibrational mode. Figure 8 shows spectra for $SH^-$ and $SD^-$ in KBr at three different temperatures. (The few extremely sharp features superimposed on these sidebands are associated with small concentrations of other impurities.) In each sample the low frequency phonon-induced sideband absorption increases as the temperature increases but at the same time the mode at the

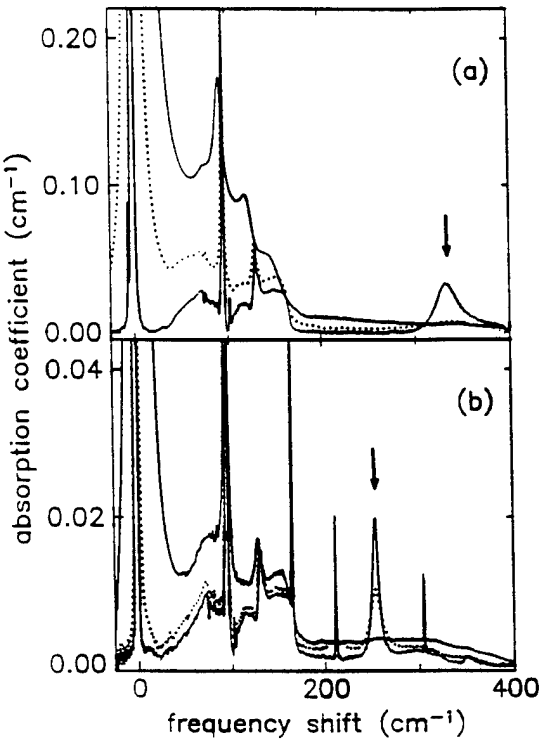


Figure 8. Absorption spectrum of the vibrational modes and sidebands for $SH^-$ and $SD^-$ in KBr. The temperature is 1.7 K and the resolution is 1 $cm^{-1}$. (a) $SH^-$; (b) $SD^-$. In each case the stretch mode is at zero frequency. The broad absorption band is associated with the defect activated phonon contribution. The high frequency mode that disappears with increasing temperature is identified by the arrow.

highest frequency (identified by an arrow) decreases in strength. Since this is the librational mode and since the mode has vanished by 100 K it would appear that at high temperatures the vibrational lifetime woulod be much longer than at low temperatures. Although a slight increase in the lifetime is seen with increasing tempertature, it is no where near large enough to be compatible with the fact that the mode disappears since that should shift the lifetime data into the microsecond range as represented by the room temperature $CN^-$ data shown in Fig. 6(b).

### C. Vibrational relaxation of diatomic molecules in glass

For small matrix isolated molecules, persistent hole burning[72] and photon echo[73] experiments probe the dephasing of vibronic excitations, while transient saturation experiments[74] can be used to extract the energy decay time. The transfer of vibrational energy from small molecules to the condensed matter host is a topic of increasing experimental activity since decay times differing by many orders of magnitude have been found. Of particular current interest are the relaxation properties of molecules in glassy hosts, where both the effect of site dependent disorder and the dynamics of amorphous systems can be studied. Short times (subnanosec) have been reported for the OH stretch mode in fused silica, where a decay process into 4 lower frequency vibrational modes of the glass has been proposed[75]. Here we describe our IR pump-probe measurements for a related small molecule-covalent glass system: the SH stretch mode in $As_2S_3$ glass.

The measurement of the vibrational relaxation time of the SH stretch mode in hydrogenated $As_2S_3$ glass provides an important test of the earlier OH-fused silica multi-quanta hypothesis. Due to the lack of high frequency excitations in the $As_2S_3$ glass[76], at least 7 vibrational quanta are required to match the SH stretch mode energy. Thus, a longer lifetime is expected for a relaxation due to a 7th order process compared to the 4th order process for OH doped silica glass if the lifetime depends mainly on the order of the relaxation mechanism.

A further reason for this study relates to the earlier persistent infrared hole burning measurements on the SH stretch mode in hydrogenated $As_2S_3$ glass samples at low temperatures[77]. This study revealed a strong frequency dependence of the persistent hole width within the inhomogeneously broadened SH absorption band. The proposed explanation for the variable relaxation time is a frequency dependent coupling of the stretch mode vibration to the matrix. The total dephasing time $T_2$ is given by Eq. 3. Although persistent hole burning experiments provide information about the total dephasing time only, the decay time can be estimated with the additional assumption that there are no other dynamical processes such as spectral diffusion[18] and that the energy relaxation time determines the homogeneous line width at low temperature. The obvious advantage of performing picosecond pump-probe measurements is the direct measurement

of the pure energy relaxation time $T_1$, which allows us to test the proposition that pure dephasing does not contribute to the hole width at low temperature.

A picosecond infrared pump-probe saturation technique is used to determine the energy relaxation rate $T_1$. A strong IR pump pulse excites a fraction of the SH oscillators to the first excited n = 1 vibrational state. Due to anharmonicity of the mode, the $n \geq 2$ transition is not resonant with the pump pulse, thus the population in the first vibrational level leads to a bleaching of the absorption. After the excitation, the population returns to its equilibrium value due to the relaxation of the excited vibrational state with a time constant $T_1$. The relaxation is probed by a weak probe pulse as a function of a delay $\Delta t$ between the pump and probe pulse. Denoting the intensity of the transmitted probe pulse as a function of the delay $I(\Delta t)$ and the transmitted probe intensity of the non-saturated sample $I_0$, we find for the relation between the transmitted probe intensity and the relaxation time: $\ln(I(\Delta t)/I_0) \propto \exp(-\Delta t/T_1)$.

Figure 9 displays the experimental pump-probe setup. Tunable IR picosecond laser pulses, resonant with the SH (0 -> 1) transition, are generated by difference mixing the radiation of a modified Continuum PD10 dye laser and a Continuum PY61 active-passive mode locked YAG laser in a $LiNbO_3$ crystal. Energies of about 10 μJ per pulse are obtained at 2500 $cm^{-1}$. Care was taken to adjust the linewidth (FWHM) of the IR pulse, averaged over many laser pulses, to a value of about 4

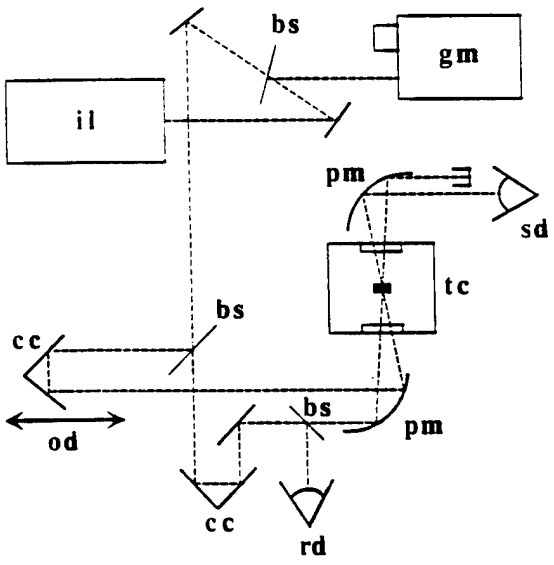


Figure 9. Experimental infrared pump-probe setup. The following abbreviations are used: bs: beamsplitter; cc: cube corner reflector; gm: grating monochromator with InSb detector; il: infrared laser system; od: optical delay line; pm: parabolic mirror; rd: reference detector; sd: signal detector; tc: temperature variable cryostat.

$cm^{-1}$. The length of the infrared pulses is 15 psec and the repetition rate of the laser system is 10 Hz. A small fraction of the pulse is coupled into a monochromator equipped with an InSb detector to monitor the frequency. The main IR pulse is focused on the sample by means of an off-axis gold coated parabolic mirror. The saturation ( < 5%) of the SH absorption line is measured by a weak probe beam, split off from the main pump pulse, delayed with respect to the pump pulse on an optical delay line and detected by a thermoelectrically cooled PbSe detector, mounted on an integrating sphere. The sample is mounted on the cold finger of a temperature variable cryostat. To ensure a good thermal link, the 2 mm thick sample, cut and polished from a hydrogenated $As_2S_3$ ingot, is attached with indium to the copper block of the sample holder. The sample temperature is monitored by a calibrated carbon resistor.

The SH doped samples are prepared by melting pure $As_2S_3$ glass in a sealed quartz tube filled with hydrogen gas at one atmosphere. Upon first heating the tube to 500 C for 30 minutes and then air quenching, a strong stretch mode band is produced. The solid line in Fig. 10 shows the absorption spectrum of the hydrogenated $As_2S_3$ sample in the region of the SH absorption band at 1.5 K, with an absorption maximum at 2485 $cm^{-1}$. The width of the inhomogeneously broadened line is about 100 $cm^{-1}$, reflecting the influence of the disordered host on the stretch mode frequency. Low temperature relaxation times were measured at a sample temperature of 8 K in the frequency range between 2425 $cm^{-1}$ and 2505 $cm^{-1}$. The results are represented by solid circles in Fig. 10. We

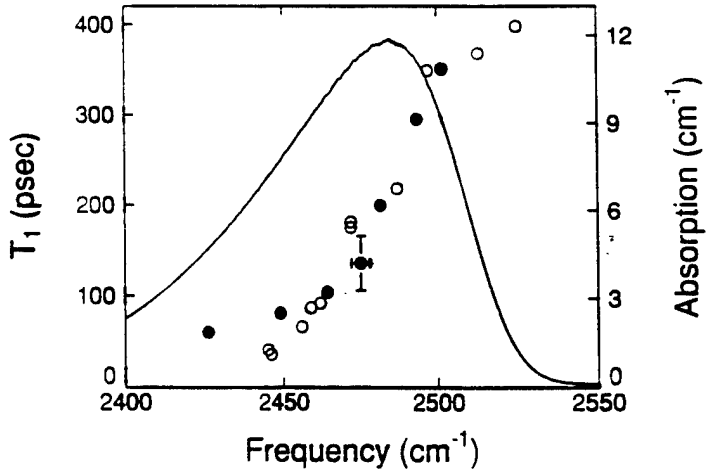


Figure 10. Frequency dependence of the lifetime of the SH stretch mode in $As_2S_3$ glass as determined by two different spectroscopic techniques. Solid circles: measured using psec pump-probe technique (8K). Open circles: lifetime extracted from hole burning results (1.5 K) obtained from Ref. [77]. The solid line represents the IR absorption coefficient (right scale) produced by SH.

find a frequency dependent lifetime that varies from 60 psec at 2425 $cm^{-1}$ to 350 psec at 2502 $cm^{-1}$. Due to inadequate absorption, no relaxation times could be measured at lower or higher frequencies. Compared to the vibrational frequency of the free SH molecule at 2599 $cm^{-1}$ [78], the frequencies of the SH molecules in the host are red shifted, which is the case when the coupling of the excited molecule to the host is stronger than that of the molecule in the ground state[78]. Thus, an SH molecule with a stretch mode at the high frequency side of the band is less strongly coupled than a molecule in the low frequency wing. We find that the decrease in the vibrational lifetime is directly related to an increased coupling to the glassy host. Also plotted in Fig. 3 are data extracted from the earlier hole burning experiments of Ref. [77] (open circles), measured at a sample temperature of 1.5 K. The plotted lifetimes are obtained under the assumption that the hole width at low temperature is determined by the energy relaxation time $T_1$. The good agreement between the two data sets shows that this assumption is indeed justified and that no other dynamical processes such as spectral diffusion are obscuring the persistent hole burning results.

The temperature dependence of the lifetime has been determined at three frequencies, 2466 $cm^{-1}$, 2494 $cm^{-1}$ and 2503 $cm^{-1}$. For all the tested frequencies, the relaxation times remain constant up to a temperature of 90 K within the error of the experiment. At higher temperature the decay rate increases gradually, becoming a factor 4 larger at room temperature. As expected, this behaviour is quite different from the temperature dependence of the persistent spectral hole width, which broadens quadratically due to dephasing. In the temperature range between 1.5 K and 10 K this dephasing leads to a broadening of the hole width by a factor of 10 [77].

Comparing the presented results with those found for the relaxation time of the OH stretch mode in fused silica[75], we find that the relaxation times of both are on the order of 100 psec at low temperatures, although the order of the respective decay processes is very different. Thus the fourth order decay process of OH mode in silica gives the same low temperature decay rate as the seventh order process of the SH mode in $As_2S_3$. In order to account for this similarity, the coupling constant must increase drastically from the OH-silica to the SH-chalcogenide system, even though both molecules are bonded covalently to their respective networks.

In conclusion, we have measured the frequency and temperature dependence of the nonradiative relaxation time of the first excited state of the SH vibrational mode in hydrogenated $As_2S_3$ glass. Within the inhomogeneously broadened band, a strong decrease in the low temperature lifetime is found for increased coupling to the host. Our findings agree with the frequency dependence of the low temperature line width found in persistent IR spectral hole burning experiments. The similarity of the results from both types of experiments show that the persistent hole width at low temperature is dominated by the energy relaxation time $T_1$. The temperature

dependence of the energy relaxation time can be explained within the framework of multi-vibrational relaxation, where the stretch mode relaxes into 7 quanta of the high frequency peak in the density of vibrational states of the glass network. We find a low temperature SH lifetime in the chalcogenide glass comparable to that of OH in fused silica, even though the orders of the processes are very different. This indicates that the magnitude of the coupling coefficient, not the order of the process, is the key ingredient in the decay dynamics for stretch modes of small molecules in these amorphous systems.

## D. Pocket Vibrational Modes in Crystals

The addition of low concentrations of substitutional $Ag^+$ ions to KI produces an unusual impurity induced vibrational spectrum which is the most thermally unstable known. Because of this property we have experimentally examined this system in some detail[79-83]. The temperature dependent spectrum is shown in Fig. 11. The substitutional $Ag^+$ defect gives rise to two strong

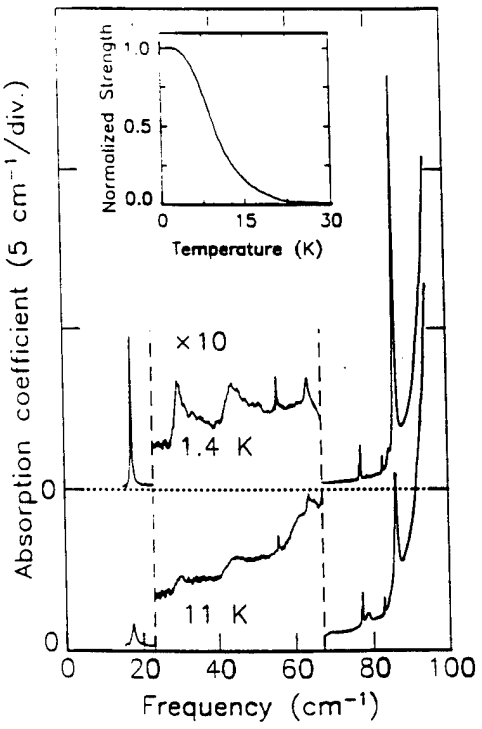


Figure 11. Absorption coefficient of KI + 0.4 mole% AgI below the reststrahl region of KI, at 1.4 K (upper trace) and 11 K (lower trace). The resolution is 0.1 $cm^{-1}$. The two spectra are displaced by a division on the ordinate axis for clarity; also, the ordinate scale in the region between 25 and 75 $cm^{-1}$ has been expanded 10× to show the weak modes in the acoustic-phonon region. The dominant features are the KI:$Ag^+$ gap and resonant modes at 86.2 and 17.3 $cm^{-1}$, respectively; additional features are identified in the text. The inset shows the temperature dependence of the strengths of the KI:$Ag^+$ features.

localized modes: a resonant mode in the acoustic phonon region, at 17.3 $cm^{-1}$, and a gap mode in the

region between the acoustic and optic phonons, at 86.2 $cm^{-1}$. Additional weak features due to $Ag^+$ at 30, 44, 55.8, and 63.6 $cm^{-1}$ (in the KI acoustic-phonon region), and at 84.5 $cm^{-1}$ (in the KI gap region) caused by $^{39}K^+ \rightarrow {}^{41}K^+$ host-lattice isotopic substitution [84], are also visible in the lower-temperature (1.4 K) spectrum. Small concentrations of other naturally-occurring impurities in these crystals give rise to additional gap modes, at 76.8 and 77.1 $cm^{-1}$ due to $Cl^-$ and at 82.9 $cm^{-1}$ due to $Cs^+$ (and another at 78.9 $cm^{-1}$, of unknown origin). In the higher-temperature spectrum of Fig. 11 (11 K), all of the $Ag^+$ features are weaker while the strengths of features associated with other defects (e.g., $Cl^-$ and $Cs^+$) remain unchanged; in addition, new features associated with the $Ag^+$ defects appear at 69 and 78.6 $cm^{-1}$. The inset of Fig. 11 shows the "universal" temperature dependence of the strengths of the KI:$Ag^+$ low-temperature configuration features, including the strong resonant and gap modes (after Ref. [85]).

Figure 12 presents the absorption coefficient of KI + 0.4 mole% AgI in the phonon gap

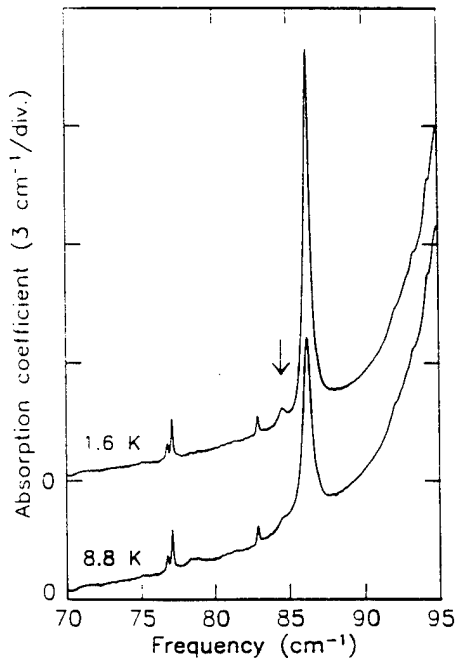


Figure 12. Impurity induced absorption coefficient of KI+0.4 mole% AgI. The restricted frequency interval covers the phonon gap region of KI. The resolution is 0.1 $cm^{-1}$. The temperature of the upper spectrum is 1.6 K, and the lower one, 8.8 K. The strong mode at 86.2 $cm^{-1}$ is the on-center KI:$Ag^+$ gap mode. This mode has lost about half its strength in the higher-temperature spectrum. The doublet at 76.8 and 77.1 $cm^{-1}$ is due to $Cl^-$ and the single peak at 82.9 $cm^{-1}$ is due to $Cs^+$. The weak temperature-dependent peak at 84.5 $cm^{-1}$ is the $Ag^+$ isotope mode. Note that the KI:$Ag^+$ modes, which have a FWHM of 0.5 $cm^{-1}$, are significantly broader than other KI gap modes, whose FWHM is ~0.14 $cm^{-1}$.

region of KI for two different temperatures at a resolution of 0.1 $cm^{-1}$. These data provide the strongest evidence for the presence of pocket modes around the defect site. The strong impurity-induced feature at 86.2 $cm^{-1}$ is the KI:$Ag^+$ gap mode corresponding to the low temperature on-center configuration of the defect system. Most of the weaker spectral features seen here and identified in the figure caption are associated with other unwanted monatomic impurities, present in either the host or dopant starting materials. When the temperature is increased from 1.6 K to 8.8 K, the strengths of this strong $Ag^+$ gap mode and a neighboring satellite line at lower frequency (identified by the arrow) are reduced in strength by a factor of two while the weak but sharp modesdue to the other impurities remain unchanged. The center frequencies of these two $Ag^+$ modes show a very small shift to lower frequencies with increasing temperature, which cannot be seen in this figure. At the highest frequencies shown in the figure, the temperature change produces an increase in the host absorption coefficient due to intrinsic difference band processes[86].

That the entire T = 0 K spectrum disappears upon heating to 25 K[84,85,87] is a result of the $Ag^+$ ion moving from the on-center configuration to an as yet incompletely determined off-center position[88]. With increasing temperature, the strengths of the (T = 0K) IR [89,90] and Raman[87] resonant mode peaks simply vanish, with a single distinguishing temperature dependence and with very little shifting or broadening. This behavior is quite different from that of systems exhibiting thermal instabilities driven by "soft" modes, whose frequencies approach zero with decreasing temperature[91]. Moreover, the observed rate at which the strengths in the KI:$Ag^+$ induced vibrational spectra disappear is much faster than can be explained by population effects associated with just the $Ag^+$ ion moving off center in a static anharmonic potential well, suggesting that the high-temperature configuration has a large number of available states of nearly the same energy as the on-center configuration[85]. This raises a number of questions: one has to do with the applicability of standard Lifshitz defect phonon theory[92-94], which assumes a single, well-isolated, potential energy minimum while another has to do with the large entropy associated with this single ion transition.

Motivated by these experimental results, we have carried out a series of detailed investigations of the T = 0 K *on-center* vibrational properties of this unusual point defect system[84,87,95]. Surprisingly, we find that despite this system's highly anomalous thermal behavior, its T = 0 K on-center dynamics are well-described by a quasiharmonic defect model, which treats anharmonic effects as perturbations. However, the experimental/theoretical comparisons have revealed several unusual properties, brand new is a novel class of impurity modes, called pocket gap modes, whose vibrational amplitudes are not peaked at the defect site but rather are highly localized on host lattice ions well-removed from the $Ag^+$ [84,96]. Figures 13(a)-

13(c) show our computed displacement patterns for gap modes of all three symmetry types. For comparison, Fig. 13(d) also shows the displacement pattern for the 17.3 $cm^{-1}$ $T_{1u}$ resonant mode, which is seen to be peaked on the impurity and its nearest neighbors. In contrast, the three gap modes consist of very similar isolated pockets of displacements on the (200) family of $K^+$ ions; hence the name pocket modes. The near degeneracy of these modes indicates that the frequencies are mainly determined by the local dynamics within each pocket, with the pockets being weakly coupled to produce the different symmetry modes. The three gap modes have some very novel properties. First, despite their different symmetries, the frequencies are very nearly degenerate. Second, the computed displacement patterns are strongly

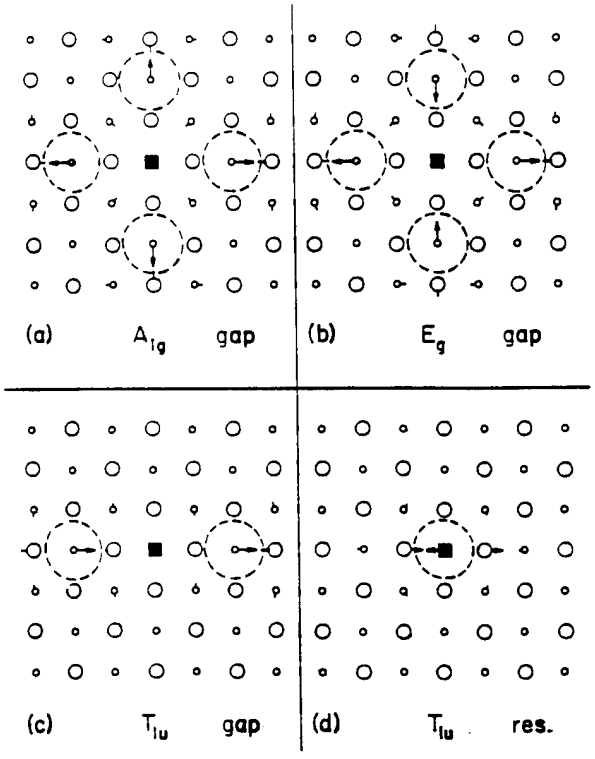


Figure 13. Expected displacement patterns for different KI:Ag+ impurity modes. (a) 87.2 $cm^{-1}$ $A_{1g}$ pocket gap mode. (b) 86.0 $cm^{-1}$ $E_g$ pocket gap mode. (c) 86.2 $cm^{-1}$ $T_{1u}x$ pocket gap mode. (d) 17.3 $cm^{-1}$ $T_{1u}x$ resonant mode. Here $T_{1u}x$ denotes the $T_{1u}$ partner which couples to x-polarized radiation, and $E_g$ denotes one of two degenerate $E_g$ partners. For our choice of partners, panels (a), (c) and (d) show displacements in the x-y plane, while (b) shows displacements in the y-z plane. Note that the displacement pattern for the resonant mode is peaked on the defect and its nearest neighbors, while the displacement patterns for the pocket gap modes (a)-(c) are peaked on the fourth neighbor sites, away from the defect.

localized on the defect's fourth neighbor (e.g. 200) potassium ions, away from the $Ag^+$ impurity and its nearest neighbors. This is in sharp contrast to the usual localized or resonant mode behavior, in which the displacement patterns are peaked at or adjacent to the defect.

In order to probe the anharmonicity associated with the KI:$Ag^+$ on-center configuration, we undertook studies of uniaxial stress[95] and dc electric field induced frequency shifts[97], both for the pocket modes, and for the low-lying impurity resonant modes[81,83] that exist below 20 $cm^{-1}$. The fact that the pocket mode displacements are sharply peaked on the (200) family of host ions renders the pocket modes sensitive to the host lattice anharmonicity near those sites, whereas the resonant modes probe the defect and its nearest neighbors. Within a quasiharmonic approach, which treats the anharmonicity perturbatively, the effect of either an applied stress or an applied E-field is to move the equilibrium positions of the ions, thereby renormalizing the harmonic force constants via the local cubic and quartic anharmonicity. The two types of experiments produce local strains of orthogonal symmetries and hence provide complementary information. We find that with the addition of $Ag^+$ electronic quadrupolar deformability to the original perturbed harmonic shell model, the predicted static electric field induced pocket gap mode frequency shifts are in good agreement with the experimental results. In addition, this new model reproduces the measured dc electric field induced frequency shifts of the KI:$Ag^+$ low-frequency resonant modes, whose measured E-field shifts are nearly two orders of magnitude larger than those for the pocket modes. The model's success, then, actually deepens the mystery surrounding the anomalous on/off center thermal instability by showing that this system's T=0 K on-center dynamics are well described by a quasiharmonic model, albeit a model which has revealed some fascinating new and unexpected behavior.

Thus based upon the successes of this study, we conclude that the $Ag^+$ electronic quadrupolar deformability play an essential role in determining the KI:$Ag^+$ on-center dynamics. Our results strongly support earlier speculations that the $Ag^+$ electronic quadrupolar deformability is an important feature in the dynamics of other host-silver defect systems and of the silver halides [98-104], including the superionic conductivity observed in AgI[102].

## E. Intrinsic Localized Vibrational Modes in Perfect Crystals

### 1. Introduction

The traditional theory of lattice dynamics, a cornerstone of solid state physics, assumes that close to the equilibrium state each atom vibrates in a harmonic potential determined by the positions of the rest of the atoms.[94,105] Starting with the Debye explanation of the low temperature specific heat of crystals and continuing up to at least the neutron diffraction measurements of lattice dispersion curves, harmonic theory and experiment have moved forward together in apparent

harmony.[91] But now the increasing number of lattice dynamics puzzles that refuse to go away suggests that the harmonic approximation and the analogous renormalized phonon model which includes weak anharmonic corrections[91,94] may not cover all of the important possibilities.

In persistent spectral hole burning experiments it is often found that the source of the photo-chemical or photo-physical persistence is unclear. Color center materials which contain simple well studied defect centers provide a good example. Even thought persistent hole burning in the zero phonon electronic transition of a color center was first observed in 1979, the proposed mechanism, photo-ionization by electron tunneling from the zero phonon line excited state to a nearby trap, has yet to be demonstrated [1]. Such apparent mysteries in this and other hole burning systems [2] have encouraged us to examine anharmonic properties of crystals to provide yet another possible mechanism for spectral persistence.

It is from this perspective that we ask the question, "What happens to the vibrational modes of a perfect one dimensional crystal when the anharmonic contribution of the interparticle interaction is comparable to the harmonic one?" It has been demonstrated that a strongly anharmonic interaction not only renormalizes the frequencies of the extended modes, but also gives rise to additional modes which are localized in space and have frequencies lying out of the plane wave phonon bands.[58,106-114] We have identified a qualitative picture of the localization mechanism for perfect anharmonic 1–D lattices which is outlined below. It also has been possible to construct an analytical description of anharmonic localized modes for realistic potential. It is easiest to start with localized modes for monatomic lattices with quartic anharmonicity. Next, the addition of cubic anharmonicity to this potential is shown to produce a new effect, that of a localized dc distortion at the local mode site. Once this has been completed nearly all of the properties of the mode have been found. Two important additions are the fact that they occur in the gap between optic and acoustic branches of the lattice and that all of these modes can move through the lattice. These modes have not yet been identified conclusively in experiment and finding them is one of the components of the present proposal.

2. Qualitative description

Consider a monatomic 1D lattice of $N$ particles, where the nearest-neighbors are connected by springs having a positive even order anharmonicity. The potential could consist of a harmonic and quartic terms in the form

$$V_{2\text{-}4}(x) = \frac{K_2}{2}x^2 + \frac{K_4}{4}x^4 \ , \qquad (6)$$

where $K_2, K_4 > 0$ and $x$ is the deviation of the spring's length from its equilibrium value. One effect of such a positive anharmonicity is to increase the frequency of each mode in the plane wave spectrum, but the eigenvectors will still extend over the entire lattice as long as the frequencies are

within the phonon band. Another effect is the localization of a vibrational mode in this perfect anharmonic lattice if the amplitude is sufficiently large with respect to those of plane waves, as the following qualitative argument illustrates[106]. The energy of $N$ independent oscillators characterized by frequency $\omega$ , mass $m$ and amplitude $u$ is $Nm\omega^2\langle u^2\rangle$, which is compared to $\hbar\omega$ in the semiclassical approximation. The rms amplitude of the vibration of a particle is then $\sqrt{\langle u^2\rangle} \sim \sqrt{\hbar / m\omega N}$. For the case of an extended mode, the number of particles vibrating within such a mode is large ( $N_{ext} >> 1$ ) so the rms amplitude at each site will be small. This need not be the case for the highest frequency mode which is not bounded from above by another mode. Since it can split off from the top of the plane wave spectrum as shown in Fig. 14(a) and become localized, it has a choice of an amplitude pattern either plane wave or localized. Which will it choose? The answer depends on the magnitude of the anharmonicity. For the localized mode case $N_{loc} \sim 1$ and the vibrating particles will have significantly larger amplitudes, which increases the effective anharmonicity of the potential and hence shifts the frequency into a forbidden region away from the plane wave spectrum. Only localized modes with imaginary Bloch wave vectors can exist in regions outside of the plane wave spectrum so given sufficient anharmonicity the localization argument is self-consistent.

Another example of the anharmonic localization of lattice vibrations can be given with a 1-D


Figure 14. Positions of the anharmonic mode frequencies relative to the plane wave dispersion curves. Case (a): When interparticle interaction has positive anharmonicity, the mode at the top of the plane waves band becomes localized. Case (b): A soft interparticle potential leads to the localization of an extended mode in the gap below the bottom of the optic band.

diatomic chain with a negative anharmonicity in the interaction between nearest-neighbors. The potential of the springs could be chosen to be that given by Eq. (1) with $K_2 > 0$ and $K_4 < 0$. Figure 14(b) illustrates the anharmonic localization of the mode that originally came from the bottom of the optic branch. In this case the localization still produces a larger amplitude at a few atoms which again increases the effective anharmonicity of the potential, but now a lower frequency results. As is the case for the monatomic lattice, the remaining modes of the lattice are plane waves with renormalized frequencies. Strictly speaking, such anharmonically driven localization of lattice vibrations is only possible when there is a frequency gap in the plane wave spectrum.

3. Monatomic lattice with cubic and quartic anharmonicity

An important discovery in how to extend the dynamical solutions to more complex potentials was made during this grant period. Previously localized modes were characterized for lattices with quartic anharmonicity in the nearest-neighbor potential. In physical systems, odd order anharmonicities are present in the Taylor's expansion of the interatomic potential, so a realistic model needs to take them into account. (It is just these terms which give rise to the thermal expansion of the lattice.) The simplest way to study anharmonic modes in a more realistic environment is to add cubic anharmonicity to the $V_{2-4}$ potential in Eq. (1) giving,

$$V_{2-3-4}(x) = \frac{K_2}{2}x^2 + \frac{K_3}{3}x^3 + \frac{K_4}{4}x^4. \qquad (7)$$

Plane wave excitations for this 1-D lattice with anharmonic nearest neighbor potentials were first studied numerically by Fermi, Pasta and Ulam.[115]

In contrast to the lattice with only quartic anharmonicity, now both odd and even harmonics are possible in the frequency spectrum as well as both ac- and dc-components of the localized mode eigenvector. After introducing the RWA displacements and solving the equations of motion, the eigenvectors and frequencies are found as a function of the cubic and quartic anharmonicity. The eigenvectors for different values of $\Lambda_3 \equiv K_3\alpha/K_2$ are presented in Fig. 15. For comparison, the odd and even eigenvector results without the cubic term are shown in Figs. 15 (a) and (c). Figures 15 (b) and (d) show that when the cubic term is included, there are again odd and even parity configurations, but the vibrations are accompanied by a localized dc expansion around the mode center and there is a slight increase in the localization of the ac amplitudes.[116] This localized dc expansion stands out as a unique property of these modes. As long as the potential contains both even and odd terms then the localized expansion follows. Associated with such a distortion is an effective mass so that when this excitation moves through the lattice the distortion and hence the mass moves with it. The resultant particle has two degrees of freedom associated with it: the internal vibrational degree and the external translational degree.

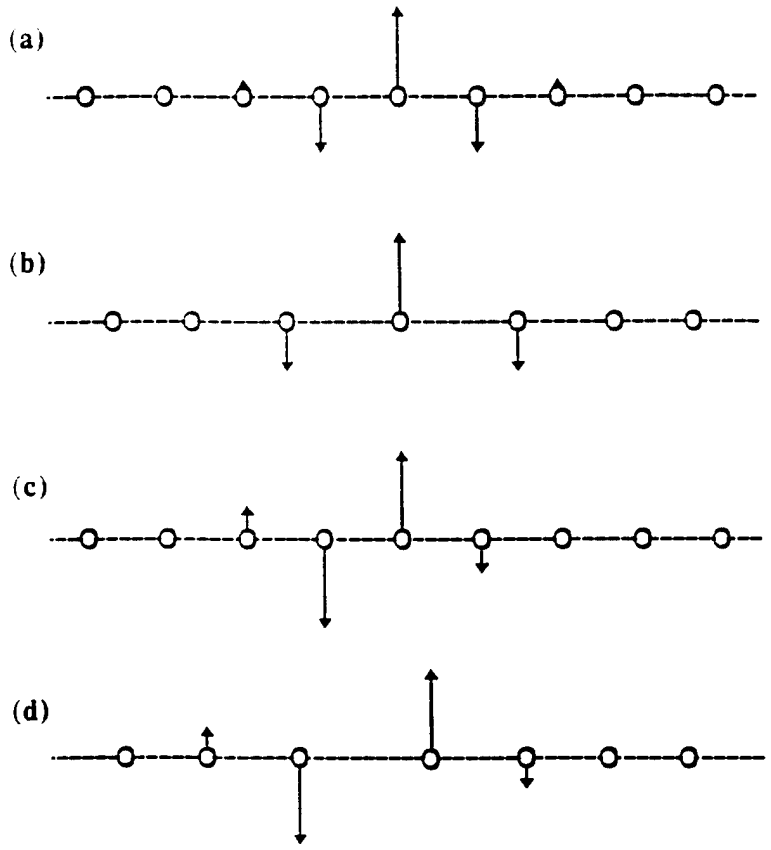


Figure 15. Vibrational amplitudes and static displacements for odd and even parity anharmonic localized modes. For convenience the arrows show the vibrational displacements perpendicular to the actual motion of the particles.

The vibrational frequency of the even parity mode is plotted in Fig. 16 as a function of the cubic anharmonicity, for several values of $\Lambda_4$. There is good agreement between the analytical frequencies (dot-dashed lines) and the results of MD simulations (open circles). For small values of $\Lambda_4$, the frequency of the localized mode decreases with increasing cubic anharmonicity until it approaches the top of the plane wave spectrum, which is represented by the horizontal dashed line. Localized modes in this transition region rapidly decay in MD simulations due to interactions with the nearby extended modes. This defines a critical cubic anharmonicity for weakly anharmonic modes, such as that characterized by $\Lambda_4 = 0.4$, beyond which localized modes are no longer stable against decay into plane wave modes.

For larger values of $\Lambda_4$, the frequency also decreases with increasing cubic anharmonicity until a different type of instability occurs. This instability arises when the interatomic potential becomes so nonlinear that a second minimum appears for sufficiently large anharmonicities.

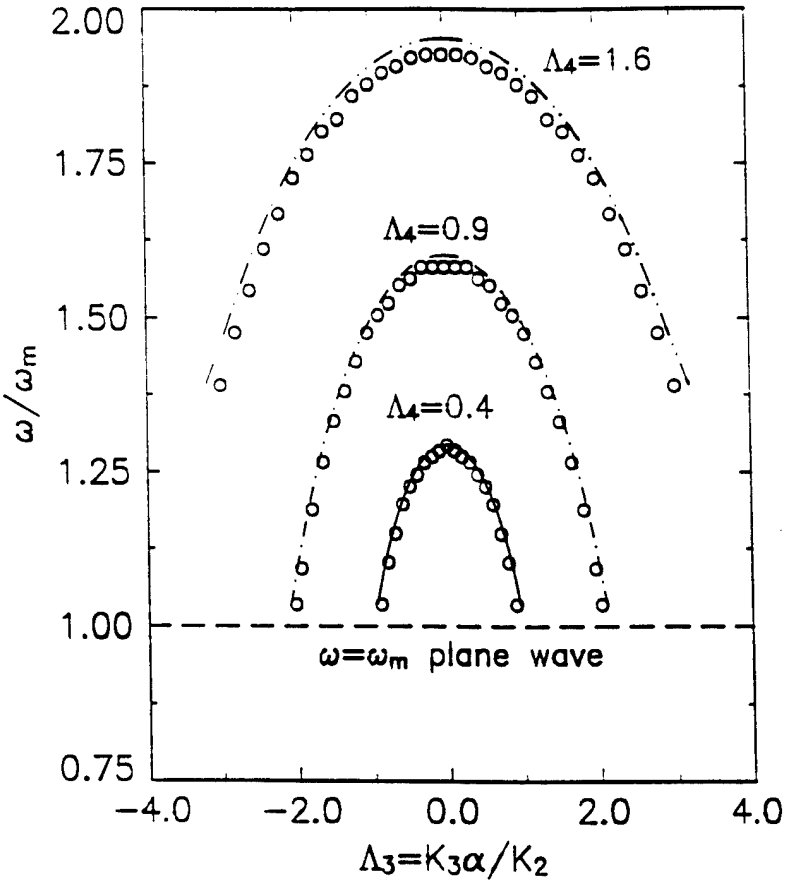


Figure 16. Frequency of even parity modes as a function of the cubic anharmonicity for three quartic anharmonicities. The curves represent analytical solutions of the equations of motion while MD simulation results are plotted as open circles.

The power spectra of the central particle's displacement in two different lattices, one with zero and the other with significant cubic anharmonicity are plotted in Fig. 17 for the same value of the quartic anharmonicity, $\Lambda_4 = 0.4$. These curves are Fourier transforms of the simulated displacements of one of the central particles of an even parity mode in a monatomic chain with 1536 particles and free end conditions. With the cubic term absent from the potential, only odd order frequency components should appear in the power spectrum, as illustrated by the dashed curve in Fig. 17. The solid curve in the same figure shows that when there is cubic anharmonicity, a zero frequency peak appears as a result of the localized dc expansion associated with the anharmonic

vibrational mode. The second and other even harmonics are also present, but with strengths that are several orders of magnitude smaller than the third harmonic. An earlier study of lattices with quartic anharmonicity shows that the frequency shift due to the third harmonic is at most 5 %, so the effect of the second harmonic will be even smaller.[111] Note that the local mode frequency for a lattice with cubic and quartic anharmonicity $[(\omega / \omega_m) = 1.12]$ is smaller than the frequency for a lattice with

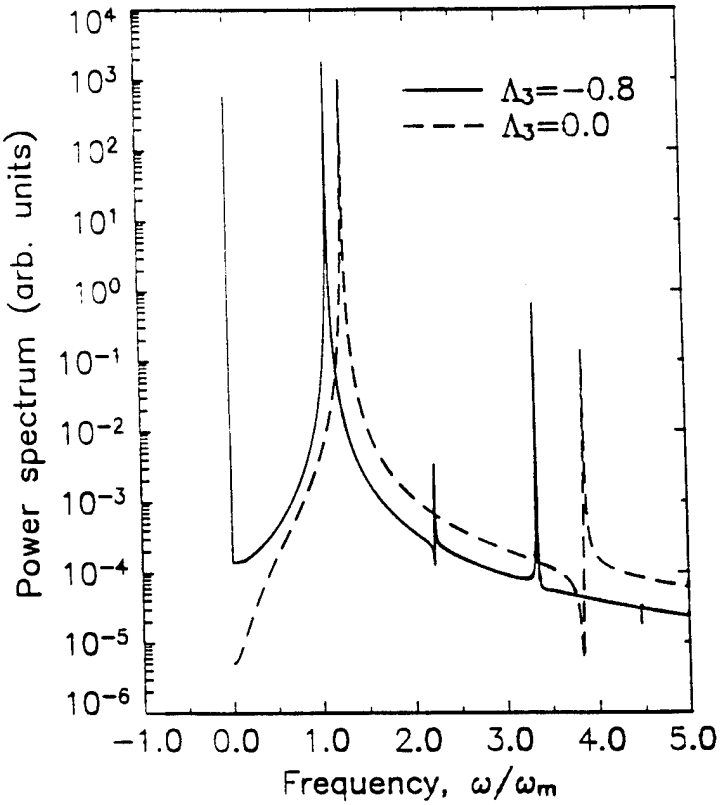


Figure 17. Power spectra of the vibrations of the central particles of an even mode in lattices with and without cubic anharmonicity. Only odd harmonic of the fundamental frequency are present in the former case (dashed curve), but a large zero frequency peak appears with the addition of cubic anharmonicity in the latter case (solid curve). In both cases, the strengths of the higher harmonic peaks are greatly reduced with respect to the fundamental, indicating that the single frequency RWA is accurate.

only quartic anharmonicity $[(\omega / \omega_m) = 1.29]$. This red shift in the vibrational frequencies is due to the softening of the interatomic potential with large amplitude displacements from equilibrium.

The illustrations above show that adding cubic anharmonicity to a nearest neighbor potential with quartic anharmonicity results in a localized dc expansion near the mode center. So far our examples of localized anharmonic vibrations have focused on stationary the modes which are formed in perfect lattices. However, because of the translational symmetry of the lattice and Bloch's theorem, they should move given the proper initial conditions. The earlier analytical framework can be expanded to include slowly moving localized modes by allowing the relative amplitudes $\xi_n$ and

$\phi_n$ to be time dependent. There is now a phase shift between the vibrations of adjacent particles of the chain, so the displacement no becomes[117]

$$u_n(t) \cong \alpha\left[\xi_n(t) + \phi_n(t)\cos(\omega t - knd)\right], \tag{8}$$

where $k$ is the wavevector of the vibrational packet. In this approach, the vibration with frequency $\omega$ is treated as an internal degree of freedom and the translational motion as an external one. This allows us to separate a "fast" and "slow" time dependence of the variables within the classical equation of motion and find the displacement and velocity patterns for the moving mode eigenvector[118].

Figure 18 presents an example of a moving localized mode in a monatomic lattice with cubic

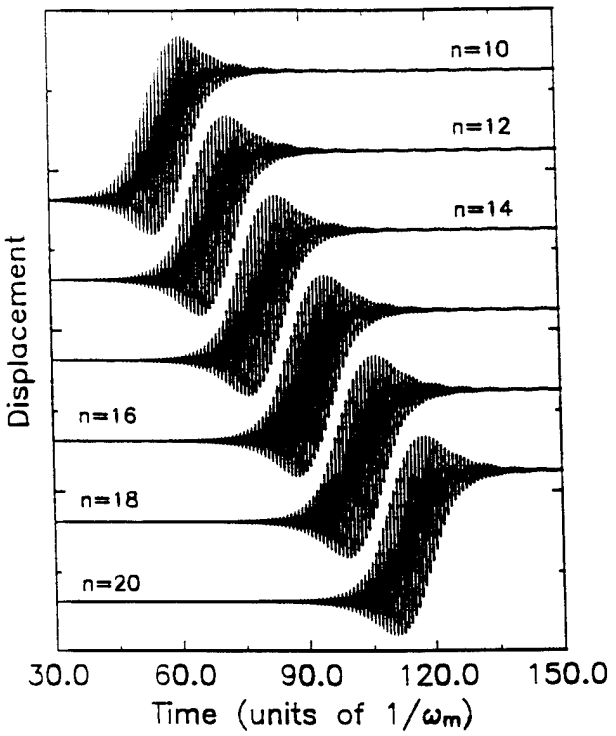


Figure 18. Displacement versus time at several sites in the monatomic chain as a localized mode moves through the lattice. The dc distortion translates rigidly with the vibrational envelope.

and quartic anharmonicity. The displacements at several lattice sites are plotted as a function of time to illustrate that the vibrational envelope and dc distortion move uniformly through the lattice. This particular mode is characterized by the same potential parameters as the stationary mode represented by the power spectrum represented by the solid curve in Fig. 17, but it now has a wave vector $kd = 0.1$. In diatomic lattices, moving anharmonic gap modes preserve all of the features considered above for moving local mode in monatomic lattices. Namely, a localized dc distortion of the lattice follows the center of the moving mode, and the parity of the moving gap mode alternates between odd and even when the localized excitation travels through the lattice[118]. A new gap mode feature

for the diatomic chain is that the light particles of the lattice have large vibrational amplitudes that are of the same order of magnitude as their dc displacements in the traveling lattice distortion. In contrast, the heavy particles of the lattice participate mainly in the translational motion of the mode, i.e. their positions follow the dc lattice distortion exactly while their ac vibrational amplitudes remain much smaller those of the light particles. In other words, the internal vibrational motion of the anharmonic gap mode is primarily on the light particles, while both light and heavy mass particles are involved in the external translational motion of the dc distortion.

## F. Uncovering Extinction Sum Rules for Particles of Arbitrary Size

### 1. Introduction

Recently, it has been demonstrated both theoretically using causality and sum rules[119] and experimentally by measuring a ZnS:diamond composite in the far IR[120] that creating squared frequencies in a specific second moment formalism is a rigorous and useful way to identify the important resonant frequencies of the electromagnetic response of a complex composite medium. The generalization of the Lyddane-Sachs-Teller relation[108] is a good example. Usually it is derived for a crystal with a diatomic crystal lattice to describe the connection between $\varepsilon_0$ the dielectric constant at low frequencies, $\varepsilon_\infty$, the dielectric constant at high frequencies, and the long wavelength lattice-optical mode frequencies in between at $\omega_l$ and $\omega_t$, but with optical moments it has a simple form even for a composite or a disordered solid such as glass. Further work by Sievers & Page[111,117] has shown that the connection between the electrodynamic and static dielectric properties of a disordered system of macroscopic size but restricted to be much less than the wavelength of light again gives characteristic second moment frequencies which replace the squared resonant frequency associated with the one mode response previously found for a small single crystal.[116] The generality of the characteristic frequency obtained for such particles although interesting has not been particularly useful because of the underlying size restriction. During the last grant period we extended these characteristic frequency ideas to a particle of arbitrary size.

### 2. Sum rules and moments for particles

The fundamental connection between the extinction cross section and the scattering matrix in the forward direction can be found in van de Hulst 1981[121]. This result, usually referred to as the optical theorem, states that

$$\mathrm{Re}\left\{\hat{C}_{ext}(\omega)\right\} = \frac{4\pi}{k^2}\,\mathrm{Re}\left\{\hat{S}(0^\circ,\omega)\right\}, \tag{9}$$

where

$$\hat{S}(0^\circ,\omega) = \tfrac{1}{2}\sum_n (2n+1)[\hat{a}_n(\omega) + \hat{b}_n(\omega)], \tag{10}$$

with $\hat{a}_n$ and $\hat{b}_n$ are the complex scattering coefficients. Detailed descriptions of the evaluation of these coefficients for different scattering problems have been given (van de Hulst 1981; Kerker 1969; Boren and Huffman 1983).[56,121,122] Since $\hat{S}(0°,\omega)$ is a causal response function and hence has its poles in the lower half complex plane, it also must satisfy the K-K relations. Boren and Huffman[56] have used this result and the connection to the extinction coefficient given by Eq. (9) to obtain a dc sum rule in terms of an integral over the extinction coefficient for a sphere. A similar procedure is used by us obtain both the dc and the oscillator-strength extinction sum rules for an ellipsoid of arbitrary size.[123] The results are

$$\frac{4\pi V}{L_i c}\left\{\frac{\eta_i(0)-\eta_{i\infty}}{\eta_i(0)}\right\} = \frac{2}{\pi}\int_0^\infty \frac{dx\ \mathrm{Re}\{\hat{C}_{ext}(x)\}}{x^2}, \tag{11}$$

and

$$\frac{4\pi V}{L_i c}\frac{\omega_p^2}{\eta_{i\infty}} = \frac{V\omega_p^2}{c} = \frac{2}{\pi}\int_0^\infty dx\,\mathrm{Re}\{\hat{C}_{ext}(x)\} \quad \text{(any size or shape particle)} \tag{12}$$

where this latter sum rule is independent of the ellipsoid depolarization factor since in free space $4\pi/L_i = \eta_{i\infty}$.

It is also possible to identify a characteristic extinction frequency for an arbitrarily sized particle. The exact result depends on whether the particle is conducting or insulating:

$$\langle\omega^2\rangle_{ext} = \frac{\omega_p^2}{\eta_{i\infty}} \quad \text{(any size conducting particle),} \tag{13}$$

$$\frac{\langle\omega^2\rangle_{ext}}{\langle\omega^2\rangle_t} = \frac{\eta_i(0)}{\eta_{i\infty}} \quad \text{(any size insulating particle).} \tag{14}$$

This last expression characterizing with a frequency the extinction behavior of an ellipsoid of arbitrary size has the same form as the generalized Fröhlich relation that relates the squared frequency characterizing the absorption behavior of an ellipsoid in the Rayleigh limit with the small particle dielectric constant. Although the extinction and absorption spectra in the large particle and small particle cases are very different, since the former includes absorption and scattering while the latter only includes absorption, it is noteworthy that Eqs. (13) or (14) apply to both. As long as the ellipsoids have the same shape then independent of volume the characteristic frequencies are the same. One can surmise that for the large particle extinction case there is as much scattering into the detector as out of it so that the scattering must average out when it is counted in the second moment representation. It also should be emphasized that the characteristic frequency for the extinction cross section has the same value as does the characteristic absorption frequency as found for the small particle Rayleigh limit. Since this characteristic extinction frequency is independent of particle size, size distributions cannot influence its value.

Althought the sum rule and second moment expressions have been derived for a homogeneous ellipsoid, they can be readily generalized to inhomogeneous particles such as coated spheres and particles in planetary atomospheres since they are based on causality regardless of the scattering details. The sum rules and second moment have been verified by Mie computation of the extinction cross-section spectra of large dielectric spheres and shells.[124] In the inhomogeneous case, the left hand side of the dc sum rule is replaced by $4\pi\alpha(0)/c$ where $\alpha(0)$ is the dc polarizibility of the particle which can be calculated from electrostatic theory, and the strength sum rule has a particularly simple form with the right hand side of Eq. (23) replaced by $\int dV\omega_p^2/c$ where the integral is over the volume of the particle.

To illustrate the sum rules and the characteristic squared frequency $\langle\omega^2\rangle_{ext}$ in the presence of inhomogeneity, we compute the frequency-dependent extinction spectra of both small and large hollow spherical shells with various inner to outer radius ratioes q. The optical properties of the bulk material are defined by a single Lorentz oscillator, that is,

$$\hat{\varepsilon}(\omega) = 1 + \frac{\omega_p^2}{\omega_0^2 - \omega^2 - i\gamma\omega} \tag{15}$$

where $\omega_p$=1.3 x $10^4$ $cm^{-1}$, $\omega_0$=$10^4$ $cm^{-1}$, and $\gamma$=$10^3$ $cm^{-1}$.

The volume-normalized extinction $\mathrm{Re}\{\hat{C}_{ext}(\omega)/V_m\}$ is plotted in Figure 19(a) for a homogeneous sphere with radii ranging from 0.01 μm to 2 μm . Both the size parameter $x_r = \omega_0 a/c$, with a the particle radius, and the relative skin depth $\delta_r/a = 1/x_r\kappa$, where κ is the imaginary part of the bulk refractive index, can be used to characterize the nature of the extinction spectrum. The size parameter at resonance $x_r$ for the homogeneous spheres in Figure 19(a) goes from 0.0628 for the smallest particle (0.01 μm) to a fairly large value of 12.57 for the largest particle (2 μm). Since the 0.01 μm particle has a large value for $\delta_r/a = 5.64$ and $x_r << 1$ at resonance, this case essentially represents the small-particle Rayleigh limit. Absorption is the dominant factor in the extinction cross section, see the solid curve in Fig. 19, which displays the resonance structure of the bulk dielectric function; however, the 2 μm particle with $x_r >> 1$ and $\delta_r/a << 1$ at resonance is in the opposite limit, now scattering is dominant and 408 partial wave coefficients are required at the highest frequency of the cross section spectrum (dot-dashed curve). Dramatic changes in the extinction spectrum occur in Fig. 19 as the sphere size changes between these two limits. Although the extinction spectrum is quite different in each case, Table 1 shows that the numerically determined sum rules and optical moment for five different cases remains unchanged, within the accuracy of the calculation.

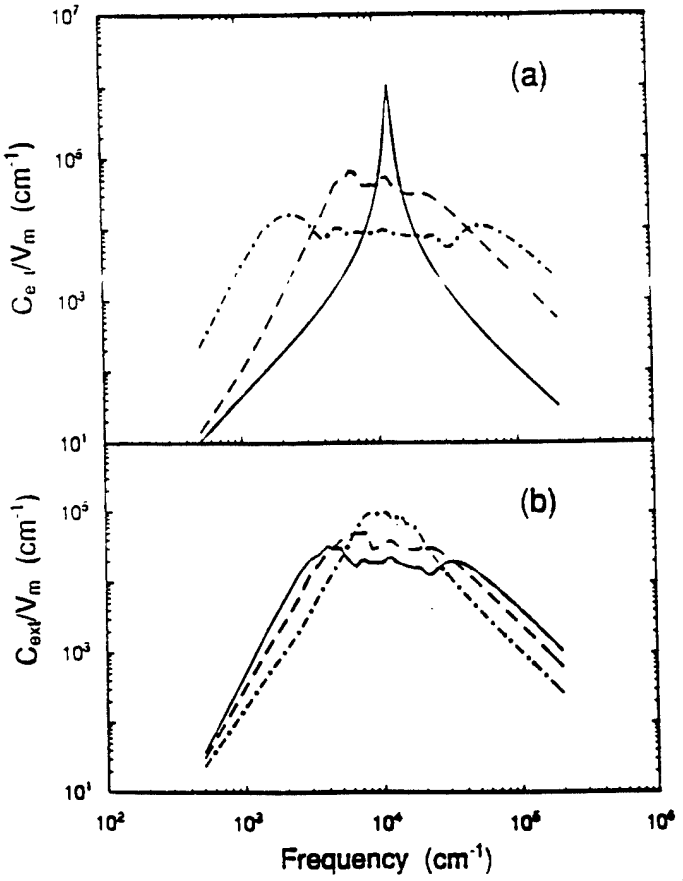


Figure 19. (a) Calculated volume-normalized extinction spectra for spheres and thin hollow spherical shells where $V = 4\pi a^3 / 3$ and a is the outer radius. Solid curves from top to bottom correspond to 0.05 μm radius spherical shells of q = 0, and 0.98, respectively. Dot-dashed curves correspond to 1.0 μm radius spherical shells of q = 0, and 0.98, respectively. q is the ratio of the inner to outer radius.
(b) The dc and strength sum rule values as functions of the inner to outer radius ratio q. The open circles and crosses indicate the numerical values calculated from the extinction spectra. The solid curves are the theoretical values which are $8\pi^2\alpha(0,q)/V$ for the dc sum rule value, and $2(1-q^3)\pi\omega_p^2$ for the strength sum rule value, respectively, with all frequencies in cm$^{-1}$. $\alpha(0,q)$ is the dc polarizibility of a spherical shell.[121]
(c) Calculated squared characteristic extinction frequency as a function of the inner to outr radius ratio q. The open circles and crosses indicate the numerical values and the solid curve is theoretical.

The stronger the scatter, the higher the frequency required in the integral to exhaust the sum rule. To see how the particle size enters in the sum rule calculation even though it does not appear in the final result, it's instructive to define an upper limit frequency $\omega_f$ to the integral which gives the fraction f (> 0.6) of the area counted. For small Rayleigh spheres, this frequency does not display a strong size dependence; however, for fairly large spheres (> 0.5 μm), where scattering is dominant, this normalized upper limit frequency for the integral $\omega_f/\omega_p = [3/(1-f)4\pi](\omega_p a/c)$ varies

linearly with the particle radius. This simple linear dependence of the upper limit of the integral follows because $\omega_f$ is in the Rayleigh-Gans scattering regime.

Figure 19(b) shows the volume-normalized extinction spectra calculated for hollow spherical shells with a fixed outer radius of a = 1 μm but different ratios, q, of inner to outer radius. The extinction spectra for particles of moderate q are similar to those for the homogeneous sphere since near resonance the radiation can not penetrate the shell to probe the hole inside. However, the extinction spectra for a sphere with q = 0.93 where the shell is penetrated near resonance displays a different response from that found for the other two cases. Although the extinction spectra shown in Figs. 19(a) and (b) are very different each other, the integrated extinction coefficient value over the spectrum is unchanged regardless of the particle size and with or without the hole.

## G. Measurement of the longitudinal asymmetry of a charged particle bunch from the coherent synchrotron or transition radiation mm-wave spectrum

In the past few years information on the bunch form factor, which is the modulus squared of the fourier transform of the longitudinal charge distribution, has been obtained for short electron bunches from spectroscopic measurements of the coherent far infrared spectrum.[125-134] It is assumed in the current analysis method that the bunch is symmetric and hence the results can not provide information about the longitudinal bunch asymmetry. In this paper we report on measurements of both synchrotron and transition far ir radiation spectra produced by submillimeter electron bunches generated with the Cornell linac and then demonstrate that with the help of a previously proposed Kramers-Kronig analysis,[135] the complete bunch shape including the longitudinal asymmetry can be determined. For experimental conditions similar to those used for injection into the Cornell synchrotron both kinds of coherent spectra give the same largely asymmetric bunch shape.

Our experiments on the bunch length shape were performed at the 2856 MHz S-band linac that serves as an injector for the Cornell storage ring. It consists of a pulsed thermoionic triode gun, a two-stage subharmonic prebuncher and a total of 8 accelerator structures, capable of producing up to $10^{11}$ electrons in a single microbunch with an energy of 300 MeV. Coherent synchrotron radiation was generated by the passage of the electrons through the field of a 0.44 Tesla bending magnet. From the geometry of the vacuum chamber of the magnet we estimate that the synchrotron spectrum is unaffected by waveguide effects for frequencies higher than 2 $cm^{-1}$. For the generation of transition radiation the bending magnet is turned off, and coherent radiation is produced by the passage of the electron bunch through the gold coated mirror. The radiation passes through a crystalline quartz window out of the vacuum chamber and is then collected by an off-axis parabolic mirror, and finally reflected off two additional flat mirrors into the spectrometer.

To analyze the spectrum of either types of radiation we use a polarizing grid Michelson spectrometer that can be remote controlled and is of rugged construction to allow extended periods of experiment without further alignment. This type of spectrometer combined with Golay cell detectors has the advantage of a fairly flat spectral response in the mm wavelength range. To correct for intensity fluctuations during the measurements, the spectrometer is equipped with an identical reference detector. The low frequency limit of the spectrometer, determined by diffraction losses and the finite aperture of the detectors, is about 2 $cm^{-1}$, the high frequency limit, determined by the grating constant of the polarizing wire beamplitters used in the instrument is about 50 $cm^{-1}$.

A measured spectrum of coherent synchrotron radiation is shown in Fig20 (a). This spectrum has been obtained with single bunch operation at a repetition rate of 15 Hz, and $2x10^9$ electrons per bunch. The linac parameters (prebuncher phase and amplitude) are similar to the standard settings used for injection into the Cornell synchrotron. Under these conditions, the electrons are present in a single bunch, as confirmed experimentally by the lack of a cross correlation signal from electrons in adjacent rf cycles of the linac. The spectrum in Fig. 20 (a) shows strong interference patterns, an indication of a structured bunch. The intensity grows rapidly with decreasing frequency, as expected for coherent radiation, and finally is suppressed below 2 $cm^{-1}$ due to the limited aperture and detector response. Figure 21(a) shows the measured coherent transition radiation spectrum under similar linac beam conditions.

To analyze these two sets of data in detail, the E-field for the coherent part of the emission spectrum is written as[136]

$$\frac{\vec{E}_{tot}(\omega)}{\sqrt{N(N-1)}} = \vec{E}_{eff}(\omega) = \hat{S}(\omega)\,\vec{E}(\omega). \tag{16}$$

so that the effective E-field at the detector is linearly related by $\hat{S}(\omega)$ to the E-field produced by an individual electron. This spectral function can be expressed as

$$ln\hat{S}(\omega) = ln\rho(\omega) + i\psi(\omega), \tag{17}$$

where $\rho(\omega)$ is the modulus and $\psi(\omega)$ is the phase factor. It can be shown that $\hat{S}(\omega)$ can be analytically continued into the complex frequency plane and that the real and imaginary parts in Eq. (17) are related by Kramers-Kronig relations.[135,137] If the form factor, $F(\omega) = S(\omega)\,S^*(\omega) = \rho^2(\omega)$, is measured at all frequencies then the frequency dependent phase factor $\psi(\omega)$ can be obtained through the following integration:

$$\psi(\omega) = -\frac{2\omega}{\pi} P\int_0^\infty dx \frac{\ln[\rho(x)/\rho(\omega)]}{x^2-\omega^2}. \tag{18}$$

With $\psi(\omega)$ known the determination of the frequency dependence of the complex form factor is complete. The desired normalized bunch distribution function is [135]

$$S(z) = \frac{1}{\pi c}\int_0^\infty d\omega\, \rho(\omega)\cos[\psi(\omega) - \frac{\omega z}{c}]. \qquad (19)$$

To extract the bunch form factor from the spectrum in Fig. 20(a) we first correct the spectral distribution for the $\omega^{2/3}$ frequency dependence of the single electron emittance. Inspection of the resulting intensity versus frequency data in Fig. 20(b) indicates that the high frequency asymptote can be readily matched to the data. Somewhat more care is required in analyzing the low frequency

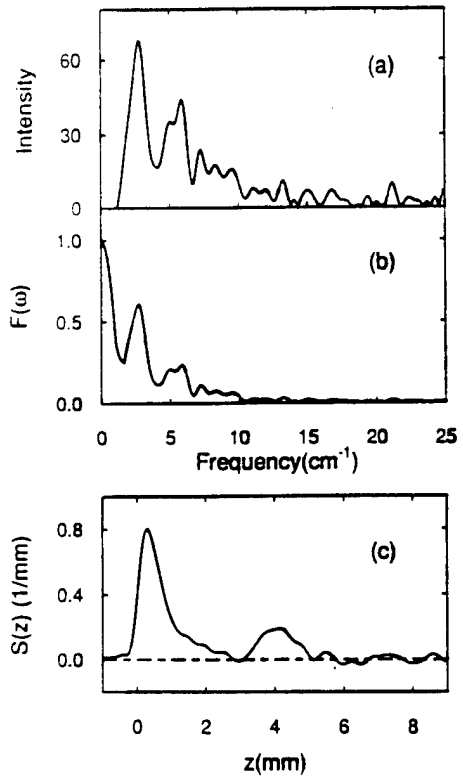


Figure 20. Measured coherent synchrotron radiation spectrum and calculated longitudinal bunch shape. The experimental beam conditions are similar to those used for injection into the Cornell synchrotron. (a) The intensity spectrum in arbitrary units is shown as a function of frequency. (b) The data in (a) are divided by $\omega^{2/3}$ then the low frequency asymtote is attached to the data between 0 and 1.6 $cm^{-1}$ with F(0) normalized to 1. (c) The calculated longitudinal bunch shape versus distance.

end of each spectrum since the intensity at the detector goes to zero while F(0) must equal one. For the spectrum with the low frequency asymptotic attachement shown in Fig. 20(b), the longitudinal bunch shape shown in Fig. 20(c) is found. The main contribution is localized in the first 1 mm with a satellite feature appearing at 4 mm.

But how much of the resulting bunch shape is a function of the low frequency attachment? As long as the asymptotic attachment occurs at low frequencies then because of the intervening

fourier transform, represented by Eq. (19), the uncertainties introduced by the low frequency details can only influence the corresponding bunch shape at large distances. The low frequency (and hence large distance) uncertainty comes from both the relative height of F(0) with regard to the measured spectrum and the frequency of the asymptotic attachment, two parameters. The normalization factor of the intensity spectrum can, in principle, be determined from the number of electrons in the bunch and the absolute intensity; however, a measurement of the absolute intensity has not yet been attempted. As we now show, neither the attachment frequency nor the relative size of F(0) have much effect on the bunch shape at small distances, the quantity of interest here.

Since the single particle emittance spectrum is flat for transition radiation, no frequency dependent correction to the data in Fig. 21(a) is required to make contact with the bunch form factor. In Figure 21(b) the results for two different relative sizes of F(0) with respect to the intensity versus frequency profile (solid and dot-dashed) are shown. Both asymptotes are attached at 1.8 $cm^{-1}$ and the resulting bunch shapes are nearly the same. Of the two parameters, the relative size of F(0) and the attachment frequency, the frequency has the largest influence on the bunch shape. Of course, to determine the exact bunch shape at large distances would require a more precise measurement at still lower frequencies. The important point here is that the main asymmetric peak in S(z) as determined from the synchrotron spectum in Fig. 20(c) or by the transition radiation spectrum in Fig 21(c) occurs at small distances (~1 mm) and is essentially uneffected by the particular asymtotic expansion that is used. Very similar shapes S(z) are found using both kinds of radiation for experimental conditions similar to those used for injection into the Cornell synchrotron.

In conclusion, the Kramers-Kronig transform technique applied to the coherent far ir spectrum produced by submillimeter charged particle bunches provides a new method for the measurement of the complete longitudinal shape. The only uncertainty in the shapes found here occurs at large distance because the lowest frequency radiation is beyond the range of the detector system, an experimental problem. For shorter bunches like those recently reported[133], this complication will vanish since in this case the low frequency form factor asymptote can be attached at a much higher frequency where the experimental uncertainties are greatly reduced.

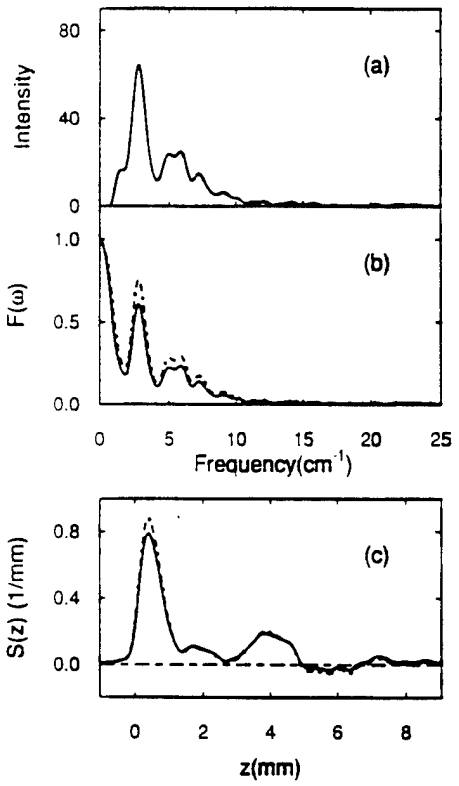


Figure 21. Measured coherent transition radiation spectrum and calculated longitudinal bunch shape. The experimental linac beam conditions are similar to those used for injection into the Cornell synchrotron. (a) The intensity spectrum in arbitrary units as a function of frequency. (b) Two different zero frequency asymtotes between 0 and 1.8 $cm^{-1}$ (solid and dashed) are attached to the low frequency data in (a). (c) The calculated longitudinal bunch shape for both cases show that the relative height of F(0) plays only a small role in fixing the exact bunch shape.

## H. Publications and Theses

(Note: A ⊕ in front of the publication indicates that the work was supported by ARO.)

⊕ "Persistent IR Hole Burning in Crystals and Glasses," A. J. Sievers, J. of Luminescence **53**, 199 (1992).

⊕ "Persistent IR Spectral Hole-Burning of the Fundamental Stretching Mode of $SH^-$ in Alkali Halides," C. E. Mungan and A. J. Sievers, J. Optical Society of America B **9**, 746 (1992).

⊕ "Vibrational Stark Effect for Matrix Isolated $CN^-$ Molecules," R. C. Spitzer, A. J. Sievers and R. H. Silsbee, J. Optical Society of America B**10**, 714 (1992).

⊕ "Persistent Infrared Spectral Hole Burning of $NO_2^-$ and $NO_3^-$ Ions in Alkali Halide Crystals: II Spectral Changes Far from the Burn Frequency," W. P. Ambrose and A. J. Sievers, J. Optical Society of America B **9**, 753 (1992).

⊕ "Persistent Infrared Spectral Hole Burning of $Tb^{3+}$ in the Glass-like Mixed Crystal $Ba_{1-x-y}La_xTb_yF_{2+x+y}$," S. P. Love, C. E. Mungan, A. J. Sievers and J. Campbell, J. Optical Society of America B **9**, 794 (1992).

⊕ "Numerical Measurements of the Shape and Dispersion Relation for Moving One-Dimensional Anharmonic Localized Modes," S. R. Bickham, A. J. Sievers, and S. Takeno, Phys. Rev. B **45**, 10344 (1992).

"Far Infrared Transmission of Superconducting $K_xC_{60}$ Films," S. A. FitzGerald, S. G. Kaplan, A. Rosenberg A. J. Sievers and R. A. S. McMordie, Phys. Rev. B **45**, 10165 (1992).

⊕ "Stress Dependence of the Pocket Gap Modes in KI:$Ag^+$," A. Rosenberg, C. E. Mungan, A. J. Sievers, K. W. Sandusky and J. B. Page, Phys. Rev. B **46**, 11 507 (1992).

"Pulsed Laser Deposition of $Ba_xSr_{1-x}TiO_3$ Thin Films," V. Mehrotra, S. Kaplan, A. J. Sievers and E. P. Giannelis, Journal of Materials Research **8**, 1209 (1993).

"Far Infrared Antiferromagnetic Resonance in $Gd_2CuO_4$," S. G. Kaplan, T. W. Noh, S-W. Cheong and Z. Fisk, Phys. Rev. B **47**, 5300 (1993).

⊕ "Pocket Vibrational Modes in Crystals: Theory and Experiment," K. W. Sandusky, J. B. Page, A. Rosenberg, C.E. Mungan and A. J. Sievers, Phys. Rev. B **47**, 5731 (1993).

⊕ "Relaxation of the Stretching Mode of Diatomic Molecules in Alkali Halides at Low Temperatures," U. Happek, C. E. Mungan, J. T. McWhirter, and A. J. Sievers, *International Conference on Defects in Insulating Materials*, O. Kanert and J.-M. Spaeth, eds., (World Scientific, 1993), p. 536.

⊕ "Pocket Vibrational Modes Due to the Silver Defect in Potassium Iodide," A. Rosenberg, C. E. Mungan, K. W. Sandusky, J. B. Page and A. J. Sievers, *International Conference on Defects in Insulating Materials*. O. Kanert and J.-M. Spaeth, eds., (World Scientific, 1993), p. 539.

⊕ "Persistent Infrared Spectral Hole Burning in the Electronic and Vibrational Spectra of Impurities," A. J. Sievers. *International Conference on Defects in Insulating Materials*, O. Kanert and J.-M. Spaeth, eds., (World Scientific, 1993), p. 102.

⊕ "Numerical Studies of the Interactions Between Moving Intrinsic Localized Modes and Defects in 1- and 2-D Anharmonic Lattices, S. R. Bickham, A. J. Sievers and S. Takeno, *International Conference on Defects in Insulating Materials*, O. Kanert and J.-M. Spaeth, eds., (World Scientific, 1993), p. 531.

⊕ "Temperature Dependence of the SeH Vibrational Dephasing Time in Chalcogenide Glasses," R. J. Till and A. J. Sievers, *Phonon Scattering in Condensed Matter VII*, R. O. Pohl and M. Meissner, eds.(Springer Verlag, New York, 1993), p. 299.

"Teraherz Phonons in Highly Disordered Crystals," U. Happek, W. W. Fischer and J. A. Campbell, *Phonon Scattering in Condensed Matter VII*, R. O. Pohl and M. Meissner, eds.(Springer Velag, New York, 1993), p. 306.

⊕ "Anharmonicity of a Thermally Unstable Lattice Defect," A. Rosenberg, B. P. Clayman, A. J. Sievers, K. W. Sandusky and J. B. Page, *Phonon Scattering in Condensed Matter VII*, R. O. Pohl and M. Meissner, eds.(Springer Velag, New York, 1993). p. .

⊕ "Comment on 'Lattice Phonon Modes in Solid $C_{60}$ Studied by Far-Infrared Spectroscopy'," S. A. FitzGerald and A. J. Sievers, Phys. Rev. Letters **70**, 3175 (1993).

⊕ "Stationary and Moving Intrinsic Localized Modes in 1-D Monatomic Lattices with Cubic and Quartic Anharmonicity," S. R. Bickham, S. A. Kiselev and A. J. Sievers, Phys. Rev. B **47**, 14 206 (1993).

⊕ "Far Infrared Sphere Resonance in a Polar Semiconductor: a Magnetooptical Study of InSb Particles," T. W. Noh, P. H. Song and A. J. Sievers, Phys. Rev B **48**, 2320 (1993).

⊕ "Anharmonic gap modes in a perfect 1-D diatomic lattice for standard two-body nearest-neighbor potentials," S. A. Kiselev, S. R. Bickham and A. J. Sievers, Phys. Rev. B **48**, 13 508 (1993).

"CO Layers on W(100) by Infrared Spectroscopy," D. M. Riffe and A. J. Sievers, Surface Science **297**, 1 (1993).

⊕ "Stationary Anharmonic Gap Modes in a One-Dimensional Diatomic Lattice with Quartic Anharmonicity," M. Aoki, S. Takeno and A. J. Sievers, J. Phys. Soc. Jpn. **62** , 4295(1993).

⊕ "Optical Moments and the Art of Dispersion Hardening," A. J. Sievers, T. W. Noh and J. B. Page, Physica A **207**, 46 (1994).

⊕ "Extinction Sum Rule and Optical Moment for an Ellipsoidal Particle of Arbitrary Size," A. J. Sievers, Optics Communication **109**, 71 (1994).

⊕ "Localized Vibrational Modes in Perfect Crystals," A. J. Sievers, S. A. Kiselev, S. R. Bickham, J. of Luminescence **58**, 37 (1994).

⊕ Ultrafast Relaxation of the Fundamental Vibration of $SH^-$ in Potassium Halides," C.E. Mungan, U. Happek, J.T. McWhirter, and A.J. Sievers, J. of Luminescence **58**, 33 (1994).

⊕ "Relaxation of the SH Vibrational Stretch Mode in $As_2S_3$ Glass," U. Happek, J.R. Engholm, and A.J. Sievers, J. of Luminescence **58**, 17 (1994).

⊕ "Localized Anharmonic Defect Modes in a 1-D Lattice with Standard Two Body Nearest Neighbor Potentials," S. A. Kiselev, S. R. Bickham and A. J. Sievers, J. of Luminescence **58**, 23 (1993).

"Relaxation of the Terahertz Phonons in Mixed Crystals Exhibiting Glass-Like Properties," W. W. Fischer, K. F. Renk, J. A. Campbell, and U. Happek, J. of Luminescence **58**, 14 (1994).

⊕ Anharmonic Impurity Modes in a 1-D lattice with Two-Body Potentials," S. A. Kiselev, S. R. Bickham and A. J. Sievers, Physics Letters A **184**, 255 (1994).

⊕ "Far IR Physics and the Processing of Optical Composites," A. J. Sievers, Proceedings of the International Conference on Millimeter and Submillimeter Waves and Applications, SPIE **2250**, 44 (1994).

⊕ Characterization of the Optical Properties of Complex Systems," A. J. Sievers, J. of Solar Energy Materials and Solar Cells **32**, 451 (1994).

⊕ "Energy transfer Between UV Generated Color Centers and the $CN^-$ Ion in Alkali Halides," J. T. McWhirter, U. Happek, and A. J. Sievers, J. of Luminescence, **60&61**, 846 (1994).

⊕ "Anharmonic Gap Mode in a 1D Diatomic Lattice with Nearest-Neighbor Born-Mayer Potentials and Its Interaction with a Mass Defect Impurity," S. A. Kiselev, S. B. Bickham and A. J. Sievers, Phys. Rev. B **50**, 9135 (1994).

⊕ "Frequency and Temperature Dependence of the Vibrational Relaxation of the SH Stretch Mode in Vitreous $As_2S_3$," U. Happek, J.R. Engholm and A. J. Sievers, Chem. Phys. Lett. **221**, 279 (1994).

⊕ "Electronic Quadrupolar Deformability and Pocket Mode Stark Effect in $KI:Ag^+$," K.W. Sandusky, A. Rosenberg, B. P. Clayman, J. B. Page and A. J. Sievers, Europhysics Letters **27**, 401 (1994).

⊕ Relaxation of the $CN^-$ Stretching Vibration in Silver Halides: The Role of Accepting Modes," U. Happek, C. E. Mungan, W. von der Osten and A. J. Sievers, Phys. Rev. Lett. **72**, 3903 (1994).

⊕ "Reassessment of millimeter-wave absorption coefficients in silicate grains," N. I. Agladze, A. J. Sievers, S. Jones, J. M. Burlich and S. V. W. Beckwith, Nature **372**, 243 (1994).

⊕ "Far-Infrared Properties of $C_{60}$ and $C_{70}$ Compacts," S. A. FitzGerald and A. J. Sievers, J. Chem. Phys. **101**, 7283 (1994).

⊕ "Determination of a Charged Particle Bunch Shape from the Coherent far IR Spectrum," R. Lai and A. J. Sievers, Phys. Rev. E **50**, R3342 (1994).

⊕ "Two-level Systems and Excited-State Transitions in Fluorite Mixed Crystals and Silica Glass," S. A. FitzGerald, J. A. Campbell, and A. J. Sievers, Phys. Rev. Letters **73**, 3105 (1994).

⊕ Measurement of the Longitudinal Asymmetry of an Electron Bunch from the Coherent Synchrotron or Transition Radiation Far IR Spectrum," R. Lai, U. Happek and A. J. Sievers, Phys. Rev. E **50**, R1 (1994).

⊕ "Two-level systems in glasses, mixed crystals and celestial solids," A. J. Sievers, S. A. FitzGerald, N. I. Agladze, J. A. Campbell, and S. V. W. Beckwith, 19th International Conference on Infrared and Millimeter Waves, K. Sakai and T. Yoneyama, eds., (Japan Society of Applied Physics, No. AP 941228, 1994), p. 275.

⊕ "Temperature Dependence of Persistent Infrared Spectral Holes for SeH Molecules in the GeAsSe Glass Series," R. Till and A. J. Sievers, J. Chem. Phys. **102**, 3077 (1995).

⊕ "Mie Computational Test of the Extinction Cross-Section Sum Rules and Optical Moments for Large Dielectric Spheres and Shells," R. Lai and A. J. Sievers, Optics Communications (1995).

⊕ "Infrared spectroscopy of the stretching modes of $SeH^-$ and $TeH^-$ in KCl and KBr: Cross sections, lifetimes and anharmonicities," C. E. Mungan, U. Happek, A. J. Sievers and T. Z. Hossain, J. Phys. Chem. Solids (1995).

⊕ "Relaxation and IR Spectroscopic Properties of the $CN^-$ Stetching Mode in Silver Halides," U. Happek, C. E. Mungan, W. von der Osten and A. J. Sievers, Proceedings of the ERODIM'94, Radiation Effects and Defects in Solids, (1995).

⊕ "Properties of Intrinsic Localized Modes in One-Dimensional Lattices," S. A. Kiselev, S. R. Bickham and A. J. Sievers, Comments in Condensed Matter Physics (1995).

⊕ "Examination of the Phase Problem Associated with the Determination of the Longitudinal Shape of a Charged Particle Bunch from its Coherent Far IR Spectrum," R. Lai and A. J. Sievers, Phys. Rev. E (1995).

⊕ "Observation of Site-Dependent Relaxation of the OH Vibrational Stretch Mode in Fused Silica, U. Happek, J.R. Engholm, and A.J. Sievers, Chem. Phys. Letters (1995).

⊕ "Unusual Anharmonic Local Mode Systems," A. J. Sievers and J. B. Page, in *Dynamical Properties of Solids*, G. K. Norton and A. A. Maradudin, eds, (North-Holland, Amsterdam, 1995), Volume 7.

⊕ "Ultrafast relaxation of the stretching modes of diatomic chalcogen hydrides in alkali halides," C.E. Mungan, U. Happek, and A.J. Sievers, Phys. Rev. B (1995).

⊕ "Laboratory Results on Millimeter-wave Absorption in Interstellar Grain Materials. I. Enstatite ($MgSiO_3$) and Forsterite ($Mg_2SiO_4$)" N. I. Agladze, A. J. Sievers, S. Jones, J. M. Burlich, and S. V. W. Beckwith, Astrophysical Journal (1995).

⊕ "Sum Rules and Optical Moments for a Scattering Medium," R. Lai and A. J. Sievers, Optical Society of America A (1995).

⊕ "Far-Infrared Studies of a Thermally Unstable Lattice Defect System," A. Rosenberg, Ph. D. Thesis, Cornell University (1993).

"Far Infrared Spectroscopy of Superconducting and Antiferromagnetic Materials," S. G. Kaplan, Ph. D. Thesis, Cornell University (1993).

⊕ "Vibrational Relaxation of Diatomic Molecules in Ionic Crystals," C. E. Mungan, Ph. D. Thesis, Cornell University (1995).

⊕ "Far Infrared Properties of Disordered Solids," S. A. FitzGerald, Ph. D. Thesis, Cornell University (1995).

## I. Participating Scientific Personnel

Faculty:

A. J. Sievers

Visiting Faculty:

John Campbell, University of Canterbury, New Zealand

Postdoctoral Associates:

N. Agladze

S. Kiselev

G. Schneider, Lynen fellow

U. Happek, Lynen fellow

B. Uebbling, Lynen fellow

Graduate Research Assistants:

S. Bickham

J. Engholm

R. Lai

C. Mungen

Undergraduate Associates:

M. Marsh

S. Smith

## III. REFERENCES


[1] S. P. Love and A. J. Sievers, in *Transport, Correlation and Structural Defects,*, edited by H. Fritzsche (World Scientific, Singapore, 1990), p. 27.

[2] W. Breinl, J. Friedrich, and D. Haarer, Chem. Phys. Lett. **153**, 379 (1984).

[3] W. S. Brocklesby, B. Golding, and J. R. Simpson, Phys. Rev. Lett. **63**, 1833 (1989).

[4] S. P. Love, A. J. Sievers, B. L. Halfpap, and S. M. Lindsay, Phys. Rev. Lett. **65**, 1792 (1990).

[5] J. C. Phillips, J. NonCryst. Sol. **34**, 153 (1979).

[6] J. C. Phillips, J. NonCryst. Sol. **43**, 37 (1981).

[7] M. F. Thorpe, J. NonCryst. Sol. **57**, 355 (1983).

[8] H. He and M. F. Thorpe, Phys. Rev. Lett. **54**, 2107 (1985).

[9] S. Feng and M. F. Thorpe, Phys. Rev. B **31**, 276 (1985).

[10] K. Tanaka, Phys. Rev. B **39**, 1270 (1988).

[11] Z. U. Borisova, *Glassy Semiconductors* (Plenum Press, 1981).

[12] K. K. Rebane and L. A. Rebane, in *Persistent spectral hole-burning: Science and applications*, edited by W.E. Moerner (Springer Verlag, Berlin, 1988), p. 17.

[13] J. M. Hayes, R. Jankowiak, and G. J. Small, in *Persistent spectral hole-burning: Science and applications,*, edited by W.E. Moerner (Springer Verlag, Berlin, 1988), p. 153.

[14] D. Haarer, in *Persistent spectral hole-burning: Science and applications*, edited by W.E. Moerner (Springer Verlag, Berlin, 1988), p. 79.

[15] R. M. MacFarlane and R. M. Shelby, J. Lumin. **36**, 179 (1987).

[16] W. M. Yen and R. T. Brundage, J. Lumin. **36**, 209 (1987).

[17] S. Völker, J. Lumin. **36**, 251 (1987).

[18] L. R. Narasimhan, K. A. Littau, D. W. Pack, Y. S. Bai, A. Elschner, and M. D. Fayer, Chem. Rev. **90**, 439 (1990).

[19] A. J. Sievers, J. Lumin. **53**, 199 (1992).

[20] P. M. Selzer, D. L. Huber, D. S. Hamilton, W. M. Yen, and M. J. Weber, Phys. Rev. Lett. **36**, 813 (1976).

[21] J. Hegarty and W. M. Yen, Phys. Rev. Lett. **43**, 1126 (1979).

[22] H. P. H. Thijssen, R. R. v. d. Berg, and S. Völker, Chem. Phys. Lett. **103**, 23 (1983).

[23] P. J. V. d. Zaag, B. C. Schokker, T. Schmidt, and R. M. MacFarlane, J. Lumin. **45**, 80 (1990).

[24] P. W. Anderson, B. I. Halperin, and C. M. Varma, Phil. Mag. **25**, 1 (1972).

[25] W. A. Phillips, Low Temp. Phys. **7**, 351 (1972).

[26] R. Silbey and K. Kassner, J. Lumin. **36**, 283 (1987).

[27] S. K. Lyo, Phys. Rev. Lett. **48**, 688 (1982).

[28] J. C. Lasjaunias, A. Ravex, and M. Vandorpe, Sol. St. Commun. **17**, 1045 (1975).

[29] S. K. Lyo and R. Orbach, Phys. Rev. B **29**, 2300 (1984).

[30] I. S. Osad'ko and A. A. Shtygashev, J. Lumin. **36**, 315 (1987).

[31] D. L. Huber, J. NonCryst. Sol. **51**, 241 (1982).

[32] D. L. Huber, in *Dynamical Processes in Disordered Materials*, edited by W.M. Yen (Transtech, 1990),

[33] U. Buchenau, N. Nücker, D. A. Dianoux, N. Ahmad, and W. A. Phillips, Phys. Rev. B **34**, 5665 (1986).

[34] J. Hegarty, M. M. Broer, B. Golding, J. R. Simpson, and J. B. MacChesney, Phys. Rev. Lett. **51**, 2033 (1983).

[35] M. M. Broer, B. Golding, W. H. Haemmerle, J. R. Simpson, and D. L. Huber, Phys. Rev. B **33**, 4160 (1986).

[36] M. Tatsumisago, B. L. Halfpap, J. L. Green, S. M. Lindsay, and C. A. Angell, Phys. Rev. Lett. **64**, 1549 (1990).

[37] S. Mahadevan and A. Giridhar, J. NonCryst. Sol. **143**, 52 (1991).

[38] A. Feltz, H. Aust, and A. Blayer, J. NonCryst. Sol. **55**, 179 (1983).

[39] K. Nandakumer and J. Phillip, in *Proceedings of the Seventh International Conference on Phonon Scattering in Condensed Matter*, edited by R.O. Pohl (Springer Verlag, Berlin, 1992), Vol. 112, p. 297.

[40] S. P. Love and A. J. Sievers, Chem. Phys. Lett. **153**, 379 (1988).

[41] S. P. Love, Ph.D. thesis, Cornell Univ., 1991 (unpublished).

[42] S. U. Nemilov, Sov, J. Phys. Chem. **37**, 1026 (1964).

[43] D. L. Huber, M. M. Broer, and B. Golding, Phys. Rev. Lett. **52**, 2281 (1984).

[44] A. Nitzan, S. Mukamel, and J. Jortner, JCP **63**, 200 (1975).

[45] H. Dubost, L. Abouaf-Marguin, and F. Legay, PRL **29**, 145 (1972).

[46] H. Dubost and R. Charneau, CP **12**, 407 (1976).

[47] Y. Yang and F. Lüty, PRL **51**, 419 (1983).

[48] T. R. Gosnell, R. W. Tkach, and A. J. Sievers, JL **31/32**, 166 (1984).

[49] T. R. Gosnell, A. J. Sievers, and R. H. Silsbee, PRL **52**, 303 (1984).

[50] T. R. Gosnell, A. J. Sievers, and C. R. Pollock, OL **10**, 125 (1985).

[51] T. R. Gosnell, R. W. Tkach, and A. J. Sievers, SSC **53**, 419 (1985).

[52] F. Lüty, CLD&AM **12**, 343 (1985).

[53] E. J. Heilweil, F. E. Doany, R. Moore, and R. M. Hochstrasser, JCP **76**, 5632 (1982). Note that the cyanide concentration was no less than 2.3 M, which corresponds to $10^{21}$ $cm^{-3}$; this is very large and hence V–V transfer processes may also be contributing to the short lifetimes. As evidence for this, they found that the times fell when the concentration was increased.

[54] J. Albertsson, S. C. Abrahams, and A. Kvick, Acta crystallographica. Section B. **45**, 34 (1989).

[55] L. Bernstein, J. C. Eilbeck, and A. C. Scott, Nonlinearity **3**, 293 (1990).

[56] M. Aoki, J. Phys. Soc. Japan **61**, 1505 (1992).

[57] M. Aoki, J. Phys. Soc. Jpn. **61**, 3024 (1992).

[58] R. Bourbonnais and R. Maynard, Phys. Rev. Lett. **64**, 1397 (1990).

[59] C. E. Mungan, U. Happek, and A. J. Sievers, JL **58**, 33 (1994). The numerical values reported in the present paper are more accurate than those reported in this and previous articles by us.

[60] C. E. Mungan, U. Happek, J. T. McWhirter, and A. J. Sievers, in *Defects in Insulating Materials*, edited by O. Kanert and J.-M. Spaeth (World Scientific, Singapore, 1993), Vol. 1, p. 536.

[61] L. E. Brus and V. E. Bondybey, JCP **63**, 786 (1975).

[62] V. E. Bondybey and L. E. Brus, JCP **63**, 794 (1975).

[63] V. E. Bondybey, JCP **65**, 5138 (1976).

[64] M. T. Bowers and W. H. Flygare, JCP **44**, 1389 (1966).

[65] H. E. Hallam, in *Vibrational Spectroscopy of Trapped Species*, edited by H.E. Hallam (Wiley-Interscience, London, 1973), p. 67.

[66] J. M. Wiesenfeld and C. B. Moore, JCP **70**, 930 (1979).

[67] L. Young and C. B. Moore, JCP **81**, 3137 (1984).

[68] D. M. Kammen, T. R. Gosnell, R. W. Tkach, and A. J. Sievers, JCP **87**, 4371 (1987).

[69] M. V. Klein, B. Wedding, and M. A. Levine, PR **180**, 902 (1969).

[70] J. Otto, StatSolB **142**, 105 (1987).

[71] U. Happek, C. E. Mungan, W. von der Osten, and A. J. Sievers, PRL **72**, 3903 (1994).

[72] W. E. Moerner, A. R. Chraplyvy, A. J. Sievers, and R. H. Silsbee, PRB **28**, 7244 (1983).

[73] D. Zimdars, A. Tokmakoff, S. Chen, S. R. Greenfield, M. D. Fayer, T. I. Smith, and H. A. Schwettmen, Rhys. Rev. Lett. **70**, 2718 (1993).

[74] A. Seilmeier and W. Kaiser, in *Topics in applied physics, Ultrashort laser pulses and applications*, edited by W. Kaiser (Springer, Berlin, 1988), Vol. 60,

[75] E. J. Heilweil, M. P. Casassa, R. R. Cavanagh, and J. C. Stephenson, CPL **117**, 185 (1985).

[76] G. Lucovsky, Phys. Rev. B **6**, 1480 (1972).

[77] S. P. Love and A. J. Sievers, CPL **153**, 379 (1988).

[78] R. S. Lowe, Mol. Phys. **41**, 929 (1980).

[79] A. J. Sievers, Phys. Rev. Lett. **13**, 310 (1964).

[80] R. D. Kirby, I. G. Nolt, R. W. Alexander, and A. J. Sievers, Phys. Rev. B **168**, 1057 (1968).

[81] I. G. Nolt and A. J. Sievers, Phys. Rev. **174**, 1004 (1968).

[82] R. D. Kirby, Phys. Rev. Lett. **26**, 512 (1971).

[83] R. D. Kirby, Phys. Rev. B **4**, 3557 (1971).

[84] K. W. Sandusky, J. B. Page, A. Rosenberg, and A. J. Sievers, Phys. Rev. B **47**, 5731 (1993).

[85] A. J. Sievers and L. H. Greene, Phys. Rev. Lett. **52**, 1234 (1984).

[86] S. P. Love, W. P. Ambrose, and A. J. Sievers, Phys. Rev. B **39**, 10352 (1989).

[87] J. B. Page, D. Schoemaker, H. Fleurent, A. J. Sievers, A. Bouwen, and J. T. McWhirter, Phys. Rev. Letters **63**, 1837 (1989).

[88] S. B. Hearon and A. J. Sievers, Phys. Rev. B **30**, 4853 (1984).

[89] S. Takeno and A. J. Sievers, Phys. Rev. Lett. **15**, 1020 (1965).

[90] R. W. Alexander, A. E. Hughes, and A. J. Sievers, Phys. Rev. B **1**, 1563 (1970).

[91] N. W. Ashcroft and N. D. Mermin, *Solid State Physics* (Saunders College, Philadelphia, 1976).

[92] I. M. Lifshitz, Nuovo Cim. Suppl. **3**, 716 (1956).

[93] A. A. Maradudin, E. W. Montroll, G. H. Weiss, and I. P. Ipatova, *Theory of Lattice Dynamics in the Harmonic Approximation*, 2nd ed ed. (Academic Press, New York, 1971), Vol. 3.

[94] H. Bilz, D. Strauch, and R. K. Wehner, *Handbuch der Physik* (Springer-Verlag, Berlin, 1984), Vol. XXV, Pt. 2d.

[95] A. Rosenberg, C. E. Mungan, A. J. Sievers, K. W. Sandusky, and J. B. Page, Phys. Rev. B **46**, 1507 (1992).

[96] K. W. Sandusky, J. B. Page, A. Rosenberg, C. E. Mungan, and A. J. Sievers, Phys. Rev. Letters **67**, 871 (1991).

[97] K. W. Sandusky, A. Rosenberg, B. P. Clayman, J. B. Page, and A. J. Sievers, Europhys. Lett. **27**, 401 (1994).

[98] K. Fischer, H. Bilz, R. Haberkorn, and W. Weber, phys. stat. sol. B **54**, 285 (1972).

[99] K. Fischer, phys. stat. sol. B **66**, 295 (1974).

[100] B. Dorner, W. v. d. Osten, and W. Bührer, J. Phys. C **9**, 723 (1976).

[101] W. G. Kleppmann, J. Phys. C **9**, 2285 (1976).

[102] H. Bilz, Cryst. Latt. Def. and Amorp. Mat. **12**, 31 (1985).

[103] P. W. M. Jacobs, J. Imaging Sci **34**, 79 (1990).

[104] J. Corish, J. Imaging Sci. **34**, 84 (1990).

[105] M. Born and K. Huang, *Dynamical Theory of Lattice Dynamics* (Oxford University Press, London, 1956).

[106] A. J. Sievers and S. Takeno, Phy. Rev. Lett. **61**, 970 (1988).

[107] S. Takeno and A. J. Sievers, Sol. St. Comm. **67**, 1023 (1988).

[108] V. M. Burlakov, S. A. Kiselev, and V. N. Pyrkov, Sol. State Comm. **74**, 327 (1990).

[109] V. M. Burlakov, S. A. Kiselev, and V. N. Pyrkov, Phys. Rev. B **42**, 4921 (1990).

[110] J. B. Page, Phys. Rev. B **41**, 7835 (1990).

[111] S. R. Bickham and A. J. Sievers, Phys. Rev. B **43**, 2339 (1991).

[112] K. W. Sandusky, J. B. Page, and K. E. Schmidt, Phys. Rev. B **46**, 6161 (1992).

[113] S. A. Kiselev, S. R. Bickham, and A. J. Sievers, Phys. Rev. B **48**, 13 (1993).

[114] C. Claude, Y. S. Kivshar, O. Kluth, and K. H. Spatchek, Phys. Rev. B **47**, 14228 (1993).

[115] E. Fermi, J. R. Pasta, and S. M. Ulam, in *Collected Works of E. Fermi*, edited by E. Segre (University of Chicago Press, Chicago, 1955),

[116] S. R. Bickham, S. A. Kiselev, and A. J. Sievers, Phys. Rev. B **47**, 14206 (1993).

[117] S. R. Bickham, A. J. Sievers, and S. Takeno, Phys. Rev. B **45**, 10344 (1992).

[118] S. A. Kiselev, S. R. Bickham, and A. J. Sievers, Physical Review B to be published (1994).

[119] T. W. Noh and A. J. Sievers, Phys. Rev. Lett. **63**, 1800 (1989).

[120] S. A. FitzGerald, T. W. Noh, A. J. Sievers, L. A. Xue, and Y. Tzou, Phys. Rev. B **42**, 5469 (1990).

[121] S. R. Bickham, A. J. Sievers, and S. Takeno, *Defects in Insulating Materials*, edited by O. Kanert and J.-M. Spaeth (World Scientific, Schloss Nordkirchen, Germany, 1993), Vol. 1, p. 531.

[122] M. Born and K. Huang, *Dynamical Theory of Crystal Lattices* (Oxford, 1954).

[123] S. Brajamani, P. S. Mazumdar, and S. K. Chowdhury, International journal of theoretical physics **30**, 487 (1991).

[124] R. Bruinsma, K. Maki, and J. Wheatley, Physical Review Letters **57**, 1773 (1986).

[125] T. Nakazato *et al.*, Phys. Rev. Lett. **63**, 1245 (1989).

[126] Y. Shibata *et al.*, Nucl. Instrum. Methods Phys. Res. Sect. A **301**, 161 (1991).

[127] E. B. Blum, U. Happek, and A. J. Sievers, Nucl. Inst. Methods Phys. Res. Sect. A **307**, 568 (1991).

[128] Y. Shibata, K. Ishi, T. Takahashi, F. Arai, M. Ikezawa, K. Takami, T. Matsuyama, K. Kobayashi, and Y. Fujita, Rhys. Rev. A **44**, R3445 (1991).

[129] U. Happek, E. B. Blum, and A. J. Sievers, Phys. Rev. Lett. **67**, 2962 (1991).

[130] K. Ishi *et al.*, Phys. Rev. A **43**, 5597 (1991).

[131] Y. Shibata, K. Ishio, T. Takahashi, T. Kanai, M. Ikezawa, K. Takami, T. Matsuyama, K. Kobayashi, and Y. Fujita, Phys. Rev. A **45**, R8340 (1992).

[132] Y. Shibata *et al.*, Phys. Rev. E **49**, 785 (1994).

[133] P. Kung, H.-C. Lihn, H. Wiedeman, and D. Bocek, Phys. Rev. Lett. **73**, 967 (1994).

[134] Y. Shibata, T. Takahashi, T. Kanai, K. Ishi, M. Ikezawa, J. Ohkuma, S. Okuda, and T. Okada, Phys. Rev. E **50**, 1479 (1994).

[135] R. Lai and A. J. Sievers, Phys. Rev. E **50**, R3342 (1994).

[136] J. S. Nodvick and D. S. Saxon, Phys. Rev. **96**, 180 (1954).

[137] F. Wooten, *Optical Properties of Solids* (Academic Press, New York, 1972).